



# Paleomagnetic study of the 1112 Ma Huanchaca mafic sills (SW Amazonian Craton, Brazil) and the paleogeographic implications for Rodinia supercontinent

Franklin Bispo-Santos<sup>a,\*</sup>, Manoel S. D'Agrella-Filho<sup>a</sup>, Renato P. de Almeida<sup>b</sup>, Amarildo S. Ruiz<sup>c</sup>, Oscar A.L. Patroni<sup>b</sup>, Julia Massucato Silva<sup>a</sup>

<sup>a</sup> Instituto de Astronomia, Geofísica e Ciências Atmosféricas, Universidade de São Paulo, Rua do Matão, 1226 São Paulo, SP 05508-090, Brazil

<sup>b</sup> Instituto de Geociências, Universidade de São Paulo, Rua do Lago, 562, Cidade Universitária, São Paulo, SP 05508-080, Brazil

<sup>c</sup> Departamento de Geologia Geral, Instituto de Ciências Exatas e da Terra, Universidade Federal de Mato Grosso, Cuiabá (MT), Brazil

## ARTICLE INFO

### Keywords:

Paleomagnetism  
Amazonian Craton  
Mesoproterozoic  
Umkondia  
Rodinia supercontinent

## ABSTRACT

During the Stenian Period (1200–1000 Ma) Rodinia was being formed, and the Amazonian Craton, presently in northern South America, was an important piece in this scenario. Recently a megacontinent named Umkondia composed by Amazonia/West Africa, Congo/São Francisco, Kalahari and India was proposed to have existed at 1100 Ma. We present a paleomagnetic study on the well-dated (U-Pb, baddeleyite) 1112 Ma mafic sills from the Huanchaca Intrusive Suite, western Mato Grosso State (Amazonian Craton) in order to test the proposed configuration of Umkondia. Alternating field (AF) and thermal stepwise demagnetization revealed northwestern characteristic remanent magnetization (ChRM) directions with low positive inclinations (mean:  $D_m = 303.2^\circ$ ,  $I_m = 12.2^\circ$ ,  $N = 10$ ,  $\alpha_{95} = 14.5^\circ$ ,  $K = 12.0$ ). A paleomagnetic pole was calculated for the Huanchaca sills ( $HU - 225.7^\circ E, 30.1^\circ N, A95 = 9.9^\circ$ ) which is classified with reliability index  $R = 5$ . Magnetic mineralogy experiments show that ChRM is carried by Pseudo single domain (PSD) magnetite. The Huanchaca paleopole favors the existence of the Umkondia megacontinent at 1100 Ma, which latter collided with Laurentia forming the Rodinia supercontinent around 1000–900 Ma.

## 1. Introduction

An important topic in ancient paleogeography is the Neoproterozoic Rodinia supercontinent (McMenamin and McMenamin, 1990). Although its existence is well-accepted, the cratonic blocks that composed it, their relative configurations and the time of final assembly are still intensively debated (Eyster et al., 2019; Jing et al., 2020, 2021; Sun et al., 2021, Evans, 2021).

There is general consensus that the Amazonian Craton was part of the Rodinia supercontinent during the early Neoproterozoic (e.g., Li et al., 2008). Geological evidence suggests that the Amazonian Craton collided with Laurentia along the 1200–900 Ma Sunsas and Grenville orogenic belts, developed along the (present day) southwestern Amazonian Craton and south to southeastern Laurentia, respectively (e.g., Brito Neves and Cordani, 1991, Sadowski and Bettencourt, 1996, among others). Most models of Rodinia shows the Amazonian Craton (together with Baltica) alongside the Appalachian-Labrador region of

Laurentia (e.g., Li et al., 2008, Johansson, 2014, Cawood et al., 2016). However, the geodynamic processes that were involved in this collision is still intensively debated, mainly due to the scarcity of paleomagnetic poles for the Stenian/Tonian Periods, and this principally for the Amazonian Craton.

Based on the 1200 Ma Nova Floresta pole (Amazonian Craton), Tohver et al. (2002) suggested an oblique collision of Amazonia with Laurentia along the Grenvillian Llanos orogen, exposed today along the coast of Texas. Thereafter, Tohver et al. (2004a, 2004b, 2005a, 2005b, 2006), based on geological, geochronological and geophysical evidence proposed that Amazonia executed a transcurrent movement relative to Laurentia up to its collision with Baltica at 1000 Ma. Later, the 1150 Ma Fortuna Formation paleomagnetic pole corroborated this model (D'Agrella-Filho et al., 2008).

Alternatively, some authors proposed that the core of the Columbia supercontinent composed of Laurentia, Baltica, the Amazonian Craton and the West Africa Craton, maintained its integrity until 1270 Ma (e.g.,

\* Correspondent author.

E-mail address: [franklin\\_bs@hotmail.com](mailto:franklin_bs@hotmail.com) (F. Bispo-Santos).

Johansson, 2009; Johansson et al., 2022). When Baltica and the Amazonian-West Africa block broke away from Columbia, they performed a clockwise rotation to again dock with Laurentia during the formation of the Rodinia supercontinent at ca. 1000 Ma ago (e.g., Johansson, 2009; Evans, 2013; D'Agrella-Filho et al., 2016; Johansson et al., 2022). Cawood and Pisarevsky (2017) also proposed a clockwise rotation of Baltica relative to Laurentia. However, these authors consider that the Amazonian Craton has never belonged to Columbia (see also Pisarevsky et al., 2014), and suggest that it collided with Laurentia at ca. 1000–950 Ma, after the closure a large ocean (named the Mirovoi Ocean).

Recently, Choudhary et al. (2019) proposed the existence of a supercraton at 1100 Ma formed by Amazonia, West-Africa, Kalahari, Congo-São Francisco and India, named by them as Umkondia. Wang et al. (2021) regarded Umkondia as a megacontinent that was essential for continental assembly. In their reconstruction, a center plume situated in the (present day) northwestern margin of the Kalahari Craton was a magmatic center from which the ca. 1100 Ma Umkondo (Kalahari), Huila-Hepembe (Congo), Mahoba (India), Huanchaca (Amazonia) and Rio Perdido (Rio Apa block) dyke swarms radiated. This megacontinent is thought to have collided with Laurentia to form Rodinia at ca. 1000–900 Ma (Choudhary et al., 2019; Wang et al., 2021).

In view of these contrasting models proposed for the collision of the Amazonian Craton with Laurentia during the assembly of Rodinia, determination of new robust paleomagnetic poles for Mesoproterozoic Amazonian geological units becomes essential to test the various models of Rodinia assembly. This work presents a new paleomagnetic pole for the well-dated 1112 Ma mafic sills from the Huanchaca Intrusive Suite (Mato Grosso State, Brazil).

## 2. Geologic setting

The Amazonian Craton is exposed in two large areas encompassing about four million square kilometers, the Guiana Shield to the north and the Central-Brazil Shield to the south, interposed by the Amazon Basin (Fig. 1a) (Schobbenhaus et al., 1984; Santos et al., 2000; Lacerda-Filho et al., 2004). According to the syntheses of Tassinari et al. (2000), Santos et al. (2003) and Cordani and Teixeira (2007), its evolution is marked by a succession of Paleo- to Neoproterozoic accretionary events with greater or lesser involvement of juvenile crust.

Based on the interpretation of geochronological data, Tassinari and Macambira (1999, 2004) proposed an evolutionary model for the Amazonian Craton, where Hadean-Archean microcontinents amalgamated through collisional Paleoproterozoic orogenies developed between 2250 Ma and 2050 Ma, followed by a succession of magmatic arcs and collisional processes that involved reactivation and reworking of pre-existing rocks. Basically, two models that subdivide the Amazonian Craton in geochronological provinces are presently available: Tassinari and Macambira (1999, 2004) and Santos et al. (2003). We adopt the Tassinari and Macambira (1999, 2004) model, which is followed by several other authors (e.g., Schobbenhaus et al., 2004; Cordani and Teixeira, 2007; Cordani et al., 2010; Bettencourt et al., 2010; Teixeira et al., 2019).

The oldest (Hadean-Archean) portion of the Amazonian Craton (Central Amazonian Province) consists of granite-greenstone terrains and high-grade metamorphic rocks exposed on the Brazil-Central and Guyana shields (Tassinari and Macambira, 2004; Nadeau et al., 2013). These are bounded by the Maroni-Itacaiunas Province developed around 2250–2050 Ma (Fig. 1a; Ledru et al., 1994).

The Hadean-Archean basement is covered by volcano-sedimentary successions with little or no deformation, ranging in age from 1980 to 1400 Ma. The southwestern part of this Hadean-Archean/Early Paleoproterozoic nucleus was accreted by subduction-related juvenile magmatic arcs, which formed the Ventuari-Tapajós (1980–1810 Ma) and Rio Negro-Juruena (1780–1550 Ma) Provinces (Fig. 1a; Tassinari and Macambira, 1999; Tassinari et al., 2000; Schobbenhaus and Brito-

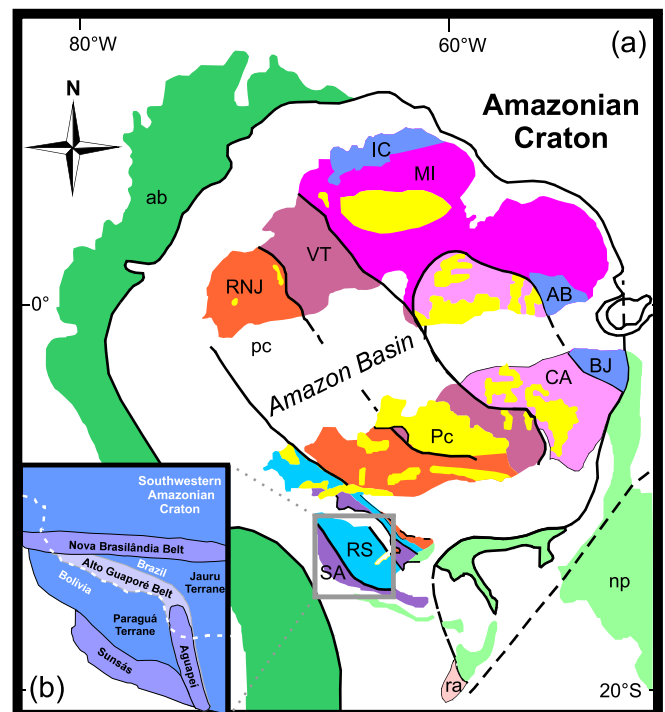


**Fig. 1.** (a) Amazonian Craton and its geologic/geochronological provinces (adapted from Cordani and Teixeira, 2007; Teixeira et al., 2019). Star indicates the study area. CA- Central Amazonian Province (>2.6 Ga); Archean partially affected in Rhyacian: IC – Imataca Complex, AB – Amapá Block, BJ – Bacajá Domain. Paleo- to Mesoproterozoic provinces: MI – Maroni Itacaiunas (2.25–2.05 Ga); VT – Ventuari-Tapajós (1.98–1.81 Ga); RNJ – Rio Negro Juruena (1.78–1.55 Ga); RO – Rondonian-San Ignacio (1.55–1.30 Ga); SA – Sunsás-Aguapeí (1.25–1.00 Ga). Ra – Rio Apa Craton; np- Neoproterozoic Provinces: ab- Andean belt; Pc- Precambrian cover; pc- Phanerozoic covers. (b) Sketch of the southwestern part of the Amazonian Craton showing the Paraguá Terrain and the Alto Guaporé, Sunsás, Aguapeí, and Nova Brasilândia belts (modified after D'Agrella-Filho et al., 2012).

Neves, 2003; Cordani and Teixeira, 2007).

During the Mesoproterozoic, magmatic arcs related to subduction processes were developed between 1600 Ma and 1300 Ma (e.g., Jauru Terrain in Mato Grosso State), which form the Rondonian-San-Ignacio Province, until the final collision of the Paraguá Terrain, about 1320 Ma ago (Fig. 1b; Bettencourt et al., 2010). This collisional model was recently extended to the northwest of the state of Rondônia, with the recognition of the Trincheira ophiolite by Rizzotto and Hartmann (2012), who interpret it as a fragment of oceanic crust raised during the Mesoproterozoic, due to the collision of the Paraguá Terrain with the proto-Amazonian Craton along the Alto Guaporé Belt (Fig. 1b).

Finally, the Sunsás collisional orogeny (the Sunsás Province) formed after 1300 Ma in the southwestern portion of Amazonia - southwestern boundary of the Paraguá Terrain (Fig. 1b). Its evolution began with a period of sediment deposition over a passive margin followed by a deformational phase at 1100–1000 Ma (Litherland et al. 1989; Sadowski and Bettencourt, 1996; Cordani and Teixeira, 2007; Teixeira et al., 2010, 2019).

As part of this scenario, is the geological evolution of the E-W Nova Brasilândia Belt or NBB (age 1100–1000 Ma) in the northern Paraguá Terrain (Fig. 1b). Contrasting interpretations consider that the NBB represents either: (i) a suture resulting from the collision between the Paraguá Terrain and proto-Amazonia together with the formation of oceanic crust and subduction processes (e.g., Tohver et al., 2005a, 2005b; Quadros et al., 2020); or (ii) intracratonic reactivations that occurred during the development of the Sunsás Belt (Sunsás Province – 1250–1000 Ma) (Litherland et al., 1989; Boger et al., 2005; Santos et al.,

2008; Teixeira et al., 2010; Cordani et al., 2010; D'Agrella-Filho et al., 2012).

The Aguapeí Belt, located in the southwest of the Mato Grosso state, represents a northern arm of the Sunsás orogeny, which is separated from the main part of the orogenesis by the Paraguá Terrain (Fig. 1b). This belt has been interpreted as an aborted continental rift, developed by sedimentary deposition of the Aguapeí Group, followed by compression and eastward thrusting at around 1000 Ma (Litherland et al. 1989; Sadowski and Bettencourt, 1996). The Aguapeí Group is stratigraphically divided into three formations, named from bottom to top as the Fortuna, the Vale da Promissão and Morro Cristalino formations (Saes and Leite, 1993; Teixeira et al., 2010; de Melo et al., 2022). Sedimentary provenance studies provided detrital zircon ages in the range  $1453 \pm 10$  Ma to  $1165 \pm 27$  Ma ( $n = 89$ ) (Santos et al., 2001; Leite and Saes, 2003) for the basal Fortuna Formation (Aguapeí Group). A more recent provenance study of the Aguapeí Group led Geraldes et al. (2014) to propose a maximum age for the sediment deposition at ca. 1265 Ma. If we consider the age of  $1149 \pm 7$  Ma as the diagenetic phase of these sedimentary rocks (D'Agrella-Filho et al., 2008), thus, the depositional age of Aguapeí Group can be between 1265 and 1150 Ma. This age is at least 40 Ma older than the Huanchaca sills (see below).

### 2.1. Huanchaca mafic sills

According to the evolutionary model established for the Amazonian Craton described above, the study area is located within the Paraguá Terrain (Fig. 1) (Tassinari and Macambira, 1999; Lima et al., 2012; Teixeira et al., 2015). This terrane is crosscut by the Rincón del Tigre mafic-ultramafic layered intrusion and the Huanchaca mafic sills

(Fig. 2a), emplaced at ca. 1112 Ma, and named the Rincón del Tigre-Huanchaca LIP (Teixeira et al., 2015, 2019; Reis et al., 2022). A component of this LIP occurs in the distal Rio Apa Terrane, known as the Rio Perdido mafic dyke swarm, and is dated at  $1110.7 \pm 1.4$  Ma (Teixeira et al., 2019).

The mafic sills from the Huanchaca Intrusive Suite (Fig. 2) emerge along the Serra Ricardo Franco or Huanchaca Hills (as it is known in the Brazilian and Bolivian territories, respectively) (Sécoco et al., 2011). In contrast to the Rincón del Tigre intrusion that was deformed by the Sunsás orogen, the Huanchaca sills were not affected by this event, as they intrude the nearly horizontal sedimentary rocks from the Vale da Promissão Formation (Aguapeí Group). The sills consist of massif gabbros and diabases, ranging from melanocratic to ultramafic, fine to medium grained, showing subophitic to ophitic textures (Lima et al., 2012, 2019). The rocks are essentially composed of plagioclase (andesine), pyroxene (augite/pigeonite, and hypersthene), amphiboles (hornblende and actinolite), opaque minerals, and with some of them also containing alkali feldspar and quartz with graphic intergrowth (Lima et al., 2019).

The Huanchaca Suite is represented by two sills that emerge in the form of the stock and slab rocks intruded in the Vale da Promissão Formation sedimentary rocks. The largest body is about 50 m thick. The second mafic body is less expressive and is located in the extreme south of the study area. The contacts with the hosted rocks are always abrupt, parallel to the bedding plane, with no features of thermal metamorphism being recognized (Lima et al., 2012).

$^{40}\text{Ar}/^{39}\text{Ar}$  isotopic data yielded ages (plateaus) of  $1040 \pm 40$  Ma for amphibole and  $948 \pm 5$  Ma for plagioclase (Lima et al., 2012). Lima et al. (2019) published new  $^{40}\text{Ar}/^{39}\text{Ar}$  isotopic data revealing ages of

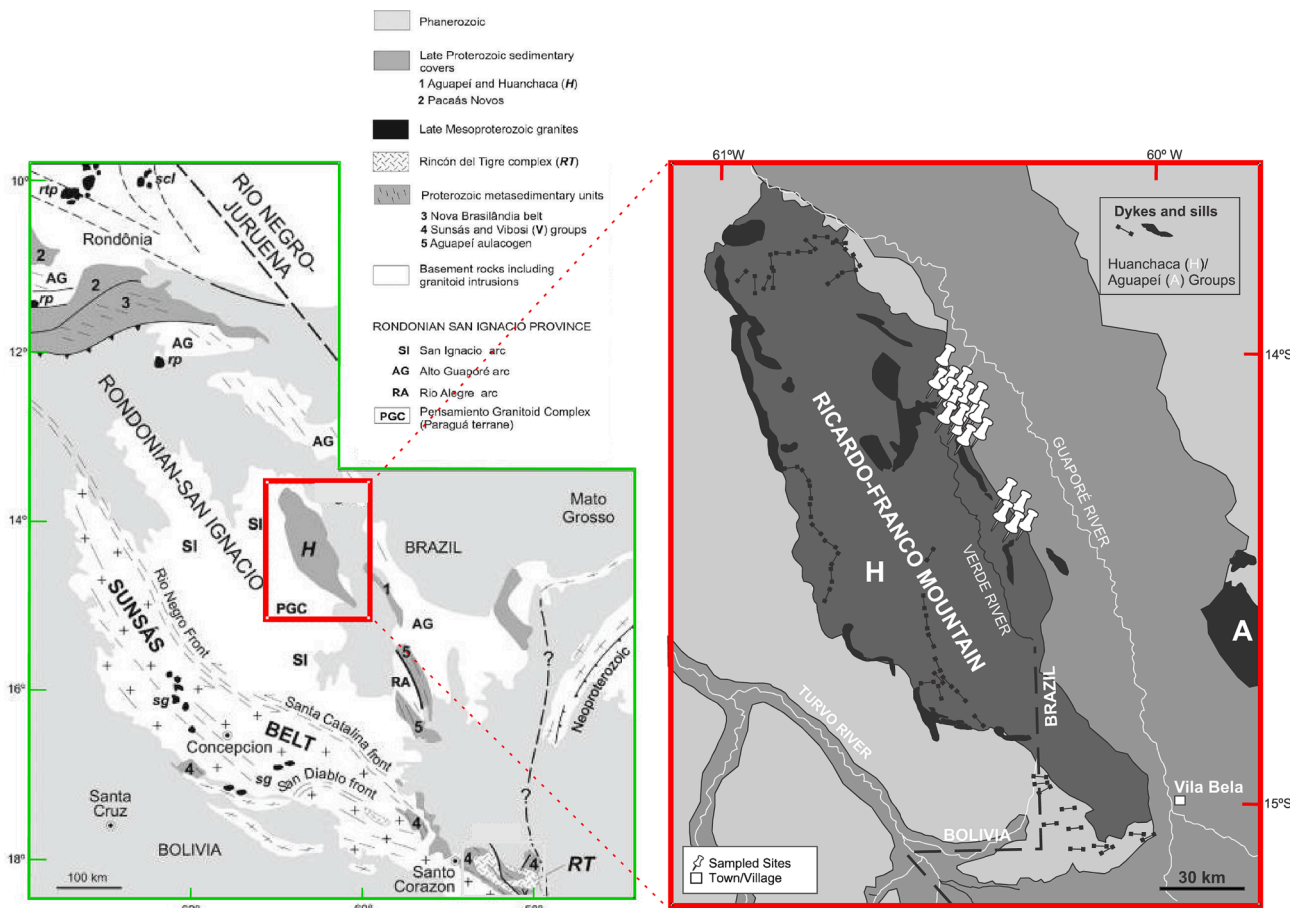


Fig. 2. Geologic sketch of the southwestern part of the Amazonian Craton (adapted from Teixeira et al., 2015). Location of the Huanchaca FRT sites are shown on the amplified figure (limited by red lines).

1041 ± 6 Ma (plagioclase – integrated age) and 1113 ± 11 Ma (amphibole, plateau age). A U-Pb (on baddeleyite) age of 1112 ± 2 Ma represents the best estimate of the crystallization of Huanchaca sills (Teixeira et al., 2015).

### 3. Paleomagnetic sampling and methods

The Huanchaca mafic sills were sampled for paleomagnetic study (Fig. 2) near the municipality of Vila Bela da Santíssima Trindade (Mato Grosso State), and Ricardo Franco or Huanchaca hills, in the Brazil-Bolivia border, southwestern Amazonian Craton. The good rock exposures allowed to collect 134 oriented cylindrical cores using a portable gas-powered drill from a total of 20 sites (Table 1).

One of the sites (FRT62) corresponds to nearly horizontal siltstones from the Vale da Promissão Formation (Aguapeí Group) sampled close to the mafic sill for a paleomagnetic baked contact test.

The cylindrical cores were oriented by sun and magnetic compasses. The sampled sites are shown in Fig. 2 and the number of cores sampled from each site and their geographic coordinates are described in Table 1.

Cylindrical cores were cut into 2.2 cm specimens. Step-wise alternating magnetic field (AF) and thermal demagnetization techniques were employed to separate the characteristic remanent magnetization (ChRM) component. Steps of 2.5 mT (up to 15 mT) and 5 mT (15 mT–100 mT) were adopted for AF demagnetization using an AF demagnetizer coupled to a cryogenic superconducting magnetometer (2G-Enterprises), model 755–4 K. Thermal demagnetization was performed using a TD-60 furnace of ASC Scientific in steps of 50 °C (from 100 °C up to 500 °C) and 20 °C (from 500 °C up to 600 °C). For samples with natural remanent magnetization (NRM) intensity stronger than 22.0 A/m, a 2-axis tumbler AGICO AF demagnetizer was used for the AF treatment and the remanent magnetization measurements were carried out using a JR-6A spinner magnetometer (AGICO, Czech Republic). These instruments are housed in a magnetically-shielded room with ambient field < 500 nT at the USPmag - paleomagnetic laboratory of the University of São Paulo.

Magnetic components for each specimen were identified in orthogonal plots (Zijderveld, 1967), and calculated using the principal component analysis (Kirschvink, 1980). At least four successive demagnetization steps were used to calculate vectors using least-squares

fits, and an upper limit for maximum angular deviation (MAD) of 8° was applied. Fisher's (1953) statistics was used to evaluate site mean directions and the paleomagnetic pole.

Magnetic mineralogy was investigated through the acquisition of remanent magnetization (IRM) using a pulse magnetizer MMPM10 (Magnetic Measurements) and hysteresis curves using a MicroMag 3900 VSM (Princeton Measurements Corporation). These curves give bulk coercive force ( $H_c$ ), coercivity of remanence ( $H_{cr}$ ), saturation magnetization ( $M_s$ ), and saturation remanent magnetization ( $M_{rs}$ ), after subtraction of the paramagnetic contribution from the high field portion of the curve. FORC (First Order Reverse Curve) diagrams were also performed for selected samples to establish domain structures. To characterize the magnetic carriers in the samples, thermomagnetic curves (low-field magnetic susceptibility versus temperature) in Argon atmosphere were performed for several samples, using a CS-4 apparatus coupled with the KLY-4S Kappabridge instrument (AGICO, Czech Republic) at the CORE laboratory in Oceanographic Institute of the University of São Paulo.

### 4. Magnetic mineralogy results

AF demagnetization showed mean destructive fields (MDF) between 4 and 10 mT for most samples (e.g., samples FRT51-A1 (site 2), FRT53-F2 (site 4), FRT63-E2 (site 10) and FRT68-C1 (site 15) in Fig. 3a), although MDF as high as 40–45 mT was also found (sample FRT55-A5, site 6) in Fig. 3a). Also, it almost completely eliminated the natural remanent magnetization (NRM) of these samples in fields up to 100 mT showing that most of the investigated sills rocks carry magnetic grains with coercivities typical of magnetite/titanomagnetite. However, NRM intensity did not decay in fields up to 100 mT for sample FRT62-E2 (site 9 - siltstones, Fig. 3a), suggesting the presence of other minerals such as hematite in this rock.

Thermal treatment indicates distributed unblocking temperature ( $T_{ub}$ ) spectra in most samples, where ca. 65% to 90% of the remanent magnetization was deleted at ~ 560 °C (Fig. 3b). In the sill samples, a steep drop in magnetization intensity between ~ 560 °C and 600 °C suggest magnetite as the main magnetic carrier. An exception is siltstone sample FRT62-E1 (site 9) where ca. 90% of NRM remained at temperatures of 600 °C, followed by a steep drop between 640 °C and 700 °C,

**Table 1**  
Huanchaca paleomagnetic data.

Site	Geographic Coordinates	Samples	Rock	Site mean direction					VGP	
				n/N	Dec (°)	Inc (°)	$\alpha_{95}$ (°)	K	Plat(°N)	Plong(°E)
1*	–14°26'22"S / –60°20'22"W	FRT50A-F	sill	16/16	230.2	67.2	2.1	312.3	–36.1	261.9
2*	–14°26'22"S / –60°20'10"W	FRT51A-D	sill	13/10	246.6	–15.1	5.1	92.1	–20.4	195.6
3	–14°26'22"S / –60°20'13"W	FRT52A-I	sill	13/7	302.9	23.6	10.9	31.6	27.6	232.2
4	–14°13'17"S / –60°26'39"W	FRT53A-I	sill	12/9	288.3	6.0	9.7	29.3	17.0	217.6
5	–14°13'19"S / –60°26'36"W	FRT54A-H	sill	19/11	121.3	15.6	13.4	12.51	32.2	209.0
6	–14°26'21"S / –60°20'14"W	FRT55A-F	sill	19/17	296.2	21.6	2.5	199.2	21.9	228.4
7	–14°26'22"S / –60°20'17"W	FRT56A-H	sill	19/19	298.2	19.2	2.8	146.3	24.2	227.8
8*	–14°13'33"S / –60°26'58"W	FRT61A-G	sill	6/6	335.2	70.5	5.1	173.6	18.2	285.2
9	–14°13'34"S / –60°27'0.7"W	FRT62A-I	siltstone	18/11	301.9	31.9	6.7	46.8	24.7	236.9
10	–14°13'19"S / –60°26'44"W	FRT63A-G	sill	11/5	334.9	10.5	20.0	15.6	58.4	245.9
11*	–14°13'37"S / –60°26'31"W	FRT64A-G	sill	7/0	–	–	–	–	–	–
12*	–14°13'13"S / –60°26'40"W	FRT65A-F	sill	5/0	–	–	–	–	–	–
13*	–14°13'15"S / –60°26'43"W	FRT66A-F	sill	6/4	163.2	62.0	19.3	23.5	57.6	142.7
14*	–14°13'15"S / –60°26'45"W	FRT67A-F	sill	6/3	294.4	75.0	17.1	52.7	–1.4	274.5
15	–14°13'14"S / –60°26'38"W	FRT68A-F	sill	15/12	300.9	24.3	4.2	110.1	25.6	231.8
16	–14°13'47"S / –60°26'17"W	FRT69A-F	sill	15/12	299.7	25.2	2.9	220.6	24.4	231.8
17*	–14°13'46"S / –60°26'19"W	FRT70A-F	sill	8/3	249.3	–36.8	15.0	68.8	–13.6	183.9
18*	–14°13'45"S / –60°26'22"W	FRT71A-F	sill	8/4	32.8	–25.1	10.9	71.4	58.1	31.7
19*	–14°13'20"S / –60°26'42"W	FRT72A-F	sill	8/7	181.1	–30.1	11.2	30.1	59.6	301.6
20	–14°13'20"S / –60°26'36"W	FRT73A-F	sill	8/6	128.5	32.2	13.6	25.4	40.5	198.5
<b>Mean</b>				<b>10</b>	<b>303.2</b>	<b>12.2</b>	<b>14.5</b>	<b>12.0</b>		
<b>HU pole</b>							<b>9.9</b>	<b>24.9</b>	<b>30.1</b>	<b>225.7</b>

n/N – number of analyzed samples/number of samples used in the mean; Dec. – declination; Inc. – inclination;  $\alpha_{95}$ , K – Fisher's confidence cone and precision parameters (Fisher, 1953); VGP – Virtual Geomagnetic Pole; Plong – Paleolongitude; Plat – Paleolatitude. \* Excluded sites from the mean.

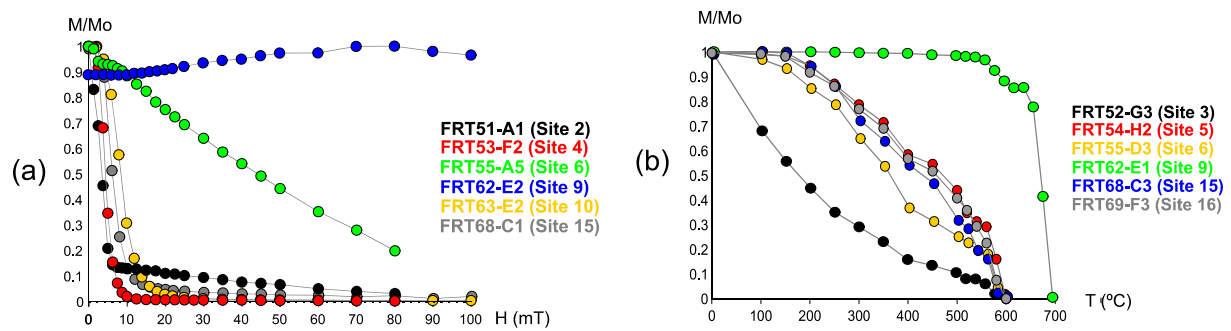


Fig. 3. Normalized magnetization intensities (M/Mo) versus (a) alternating magnetic field (H) and (b) temperature (T) for samples from different sites of Huanchaca sills and for a siltstone (site 9).

suggesting the predominance of hematite together with the presence of magnetite with  $T_{ub}$  between 540 °C and 600 °C (Fig. 3b).

The hysteresis curves obtained for the sills samples show thin waist behavior (Fig. 4a-e) indicating low coercivity minerals and saturation fields around 300 mT, typical of titanomagnetite or magnetite. Again, the exception is sample FRT62 (site 9 - siltstones) whose hysteresis curve indicates wide waist behavior with coercivity  $H_c = 145.1$  mT, suggesting predominance of hematite (Fig. 4f).

Most of these samples plots in the pseudo-domain structure (PSD) field in the Day diagram (Fig. 4g - Mrs/Ms versus  $H_{cr}/H_c$ , Day et al., 1977) modified by Dunlop (2002), which is consistent with the good magnetic stability seen in the samples after AF treatment. First order reverse curves (FORC) were obtained for selected samples to establish their domain states where magnetite/titanomagnetite predominates (Fig. 5). FORC diagrams for an ensemble of SD-particles have the shape of a symmetrical distribution of the contour along the  $B_c$  axis, without a vertical scatter along the  $B_u$  axis, and for an ensemble of PSD particles they have an asymmetric distribution with a contour moderately diverging along the vertical axis (Roberts et al., 2014). According to the FORC diagrams in Fig. 5, the magnetic minerals in the analyzed samples are in the PSD “vortex” state.

Isothermal remanent magnetization (IRM) acquisition experiments carried out for most of the Huanchaca rock samples resulted in similar behaviors with practically identical and homogeneous curves, reaching saturation magnetization in fields below 300–400 mT, indicating low coercivity grain distribution (samples FRT50 (site 1), FRT52 (site 3), FRT53 (site 4), FRT56 (site 7), FRT67 (site 14), FRT68 (site 15) and FRT69 (site 16), in Fig. 6). This behavior is typical of magnetite and titanomagnetite, corroborating the presence of these minerals as already evidenced in the previous magnetic experiments. The siltstone (FRT62, site 9) does not saturate at fields as high as 1 Tesla, indicating the presence of minerals with high coercivities, likely hematite (sample FRT62, site 9 in Fig. 6).

Reversible to moderately irreversible high-temperature thermomagnetic curves were observed for all Huanchaca sills samples, some of them indicating that probably magnetite is being formed during heating (Fig. 7). A well-characterized Hopkinson peak at around 580 °C is observed for most samples. These characteristic features are typical of thermally stable, SD/PSD Ti-poor titanomagnetite grains (Dunlop and Özdemir, 1997).

## 5. Paleomagnetic results

The NRM intensity of the Huanchaca sills samples ranges from 291 mA/m to values as high as 22.9 A/m. These intensities are typical of basaltic rocks with a high contribution of ferromagnetic minerals. On the other hand, the sedimentary rocks present NRM intensities between 850 mA/m and 1.57 A/m.

AF and thermal treatments were efficient to isolate a stable remanent magnetization for samples from most sites after eliminating random

secondary magnetic components associated with coercivities up to 15–30 mT or unblocking temperatures below 400 °C. Exceptions are the samples from sites 11 (FRT64) and 12 (FRT65), which presented magnetically unstable behavior and/or within-site inconsistent directions. Site mean directions are summarized in Table 1 and plotted in Fig. 8a.

The most representative component in the sills is characterized by northwestern positive inclination directions obtained for 9 analyzed sites. Examples of AF and thermal demagnetization are presented in Fig. 9. After demagnetization, the siltstone samples (site 9, FRT62) also revealed similar directions (Fig. 10). The site mean directions from the remaining sites are distributed in the other three quadrants in the stereogram (Fig. 8a). Trying to calculate a representative paleomagnetic pole for the analyzed sites, we considered an angle of 40° as the maximum paleosecular variation around the mean of the virtual geomagnetic poles calculated for the 18 sites in Table 1 (Fig. 8b). Although samples from sites 5 (FRT54) and 20 (FRT73) yielded southeastern directions with low positive inclinations, in our analysis we consider they registered an Earth’s magnetic field reversal. We justify this since the low magnetic inclinations imply that the Amazonian Craton was very close to Earth’s Equator and the inclination of geomagnetic field could be positive or negative during magnetic register in the rock.

Using the cutoff angle of 40°, eight sites can be excluded from the mean, resulting in a mean direction  $D_m = 303.2^\circ$ ;  $I_m = 12.2^\circ$  ( $N = 10$ ;  $\alpha_{95} = 14.5^\circ$ ;  $K = 12.0$ ) (Fig. 8c) and the corresponding paleomagnetic pole (HU pole) at  $30.1^\circ N$ ;  $225.7^\circ E$  ( $A_{95} = 9.9^\circ$ ;  $K = 24.9$ ) (Fig. 8d). Excluding site 9 represented by the sediment (siltstone), a mean direction using the 9 sills’s sites was also calculated ( $D_m = 303.3^\circ$ ;  $I_m = 9.8$ ;  $\alpha_{95} = 15.7^\circ$ ;  $K = 11.7$ ), which yielded the corresponding paleomagnetic pole at  $30.7^\circ N$ ;  $224.4^\circ E$  ( $A_{95} = 10.8^\circ$ ,  $K = 23.5$ ) (see Table 1). Since the difference of the two calculated poles is small (0.6° in latitude and 1.3° in longitude), we will consider that calculated with 10 sites as representing the Huanchaca pole (HU pole).

## 6. Discussion

### 6.1. Paleomagnetic pole reliability

The Huanchaca pole ( $30.1^\circ N$ ,  $225.7^\circ E$ ,  $A_{95} = 9.9^\circ$ ,  $K = 24.9$ ) satisfies 5 out of the 7 quality criteria proposed by Van der Voo (1990) and recently revised by Meert et al. (2020) as the R-score:

- (1) The age of the Huanchaca sills rocks can be considered well-determined by U-Pb and Ar/Ar methods. A U-Pb (baddeleyite) dating provided an age of  $1112 \pm 2$  Ma (Teixeira et al., 2015), which represents the best estimate of the sills crystallization age and probably the time their remanent magnetization was acquired. In addition, the  $1113 \pm 11$  Ma Ar-Ar plateau age obtained

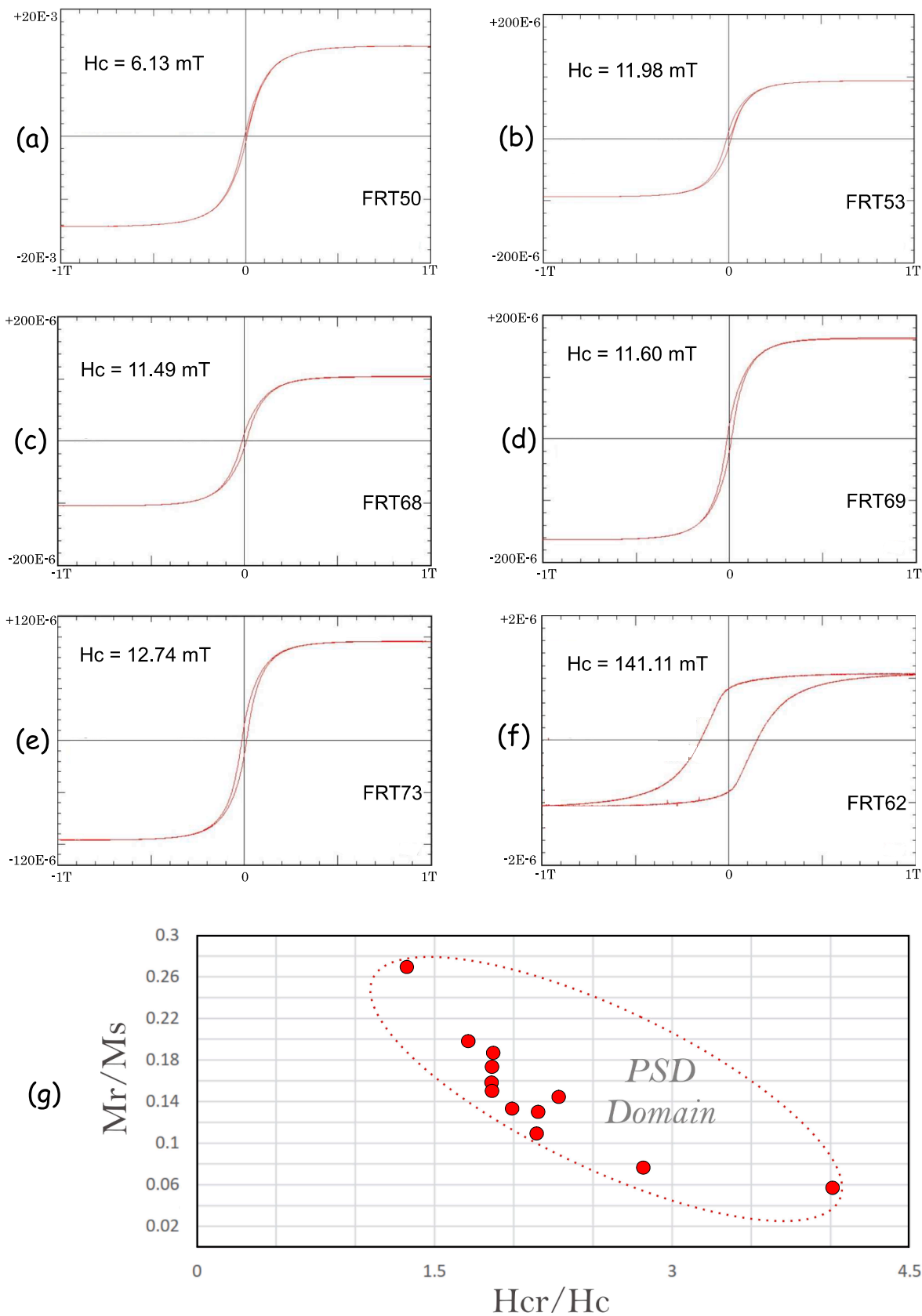


**Fig. 4.** (a, b, c, d, e): Typical narrow waist hysteresis curves (magnetic moment (Am<sup>2</sup>) versus magnetic field (T)) obtained for the Huanchaca samples, which are characteristic of titanomagnetite/magnetite minerals. (f) Wide waist hysteresis curve obtained for the siltstone sample (Vale da Promissão Formation) characteristic of hematite mineral. (g) Day's diagram suggesting the presence of PSD grains in the sill samples.

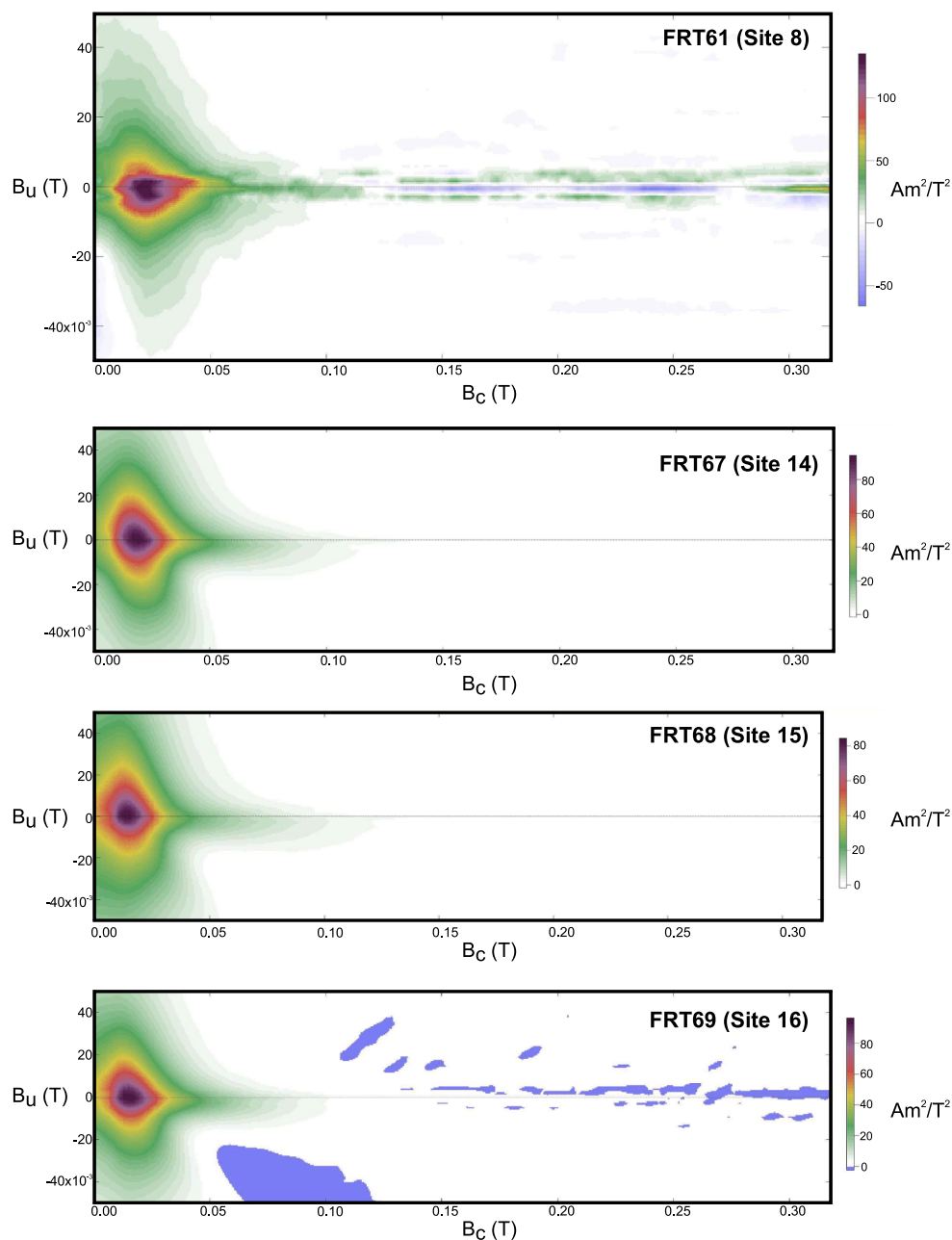


Fig. 5. FORC diagrams ( $B_u$  and  $B_c$  fields in Tesla) for selected FRT Huanchaca samples.

for amphiboles from the Huanchaca rocks (Lima et al., 2019) suggests that they experienced rapid initial cooling.

- (2) The Huanchaca pole was determined for an adequate set of samples and appropriate Fisher statistical parameters ( $A_{95} = 9.9^\circ$ ,  $K = 24.9$ ,  $N = 96$ ,  $B = 10$  sites), according to criterion R2 of Meert et al. (2020). Also, the calculated semi-angle of the Fisher's confidence cone for the HU pole ( $A_{95} = 9.9^\circ$ ) is in the expected interval ( $4.9^\circ \leq A_{95} \leq 20.5^\circ$ ) of secular variation models (Deenen et al., 2011), although the minimum number of sites used to calculate a paleomagnetic pole would need to be 15 according to these authors. In contrast, a paleolatitude of  $6.2^\circ$  was calculated for the Huanchaca magnetic inclination ( $I_m = 12.2^\circ$ ), which would imply a value of angular dispersion ( $s$ ) of ca.  $12^\circ$ - $13^\circ$ , according to Proterozoic models of secular variation (Veikkolainen and Pesonen, 2014). This is  $3.6^\circ$  lower than the  $s = 16.6^\circ$  calculated for the HU pole by equation,  $s = \left( \sum_{i=1}^N \frac{\theta_i^2}{(N-1)} \right)^{1/2}$ . A

possible reason for this discrepancy could be associated to the small number of sites carrying the HU component. Another possible reason could be related to the low Earth's magnetic field intensity in the Mesoproterozoic (Smirnov, 2017), which could enhance the Earth's non-dipole field contribution, increasing dispersion of directions.

- (3) Rock magnetic analysis, including thermomagnetic curves, IRM curves, hysteresis curves, and FORC, clearly identified PSD magnetite as the main magnetic carrier of Huanchaca component. Moreover, after AF and thermal demagnetization, magnetization components were isolated by least squares fit to the linear points observed on orthogonal diagrams, through the principal component analysis (Kirschvink, 1980);
- (4) Unfortunately, the baked contact test was incomplete, since no different magnetization direction was found for the sedimentary rocks of the Vale da Promissão Formation (Aguapeí Group).

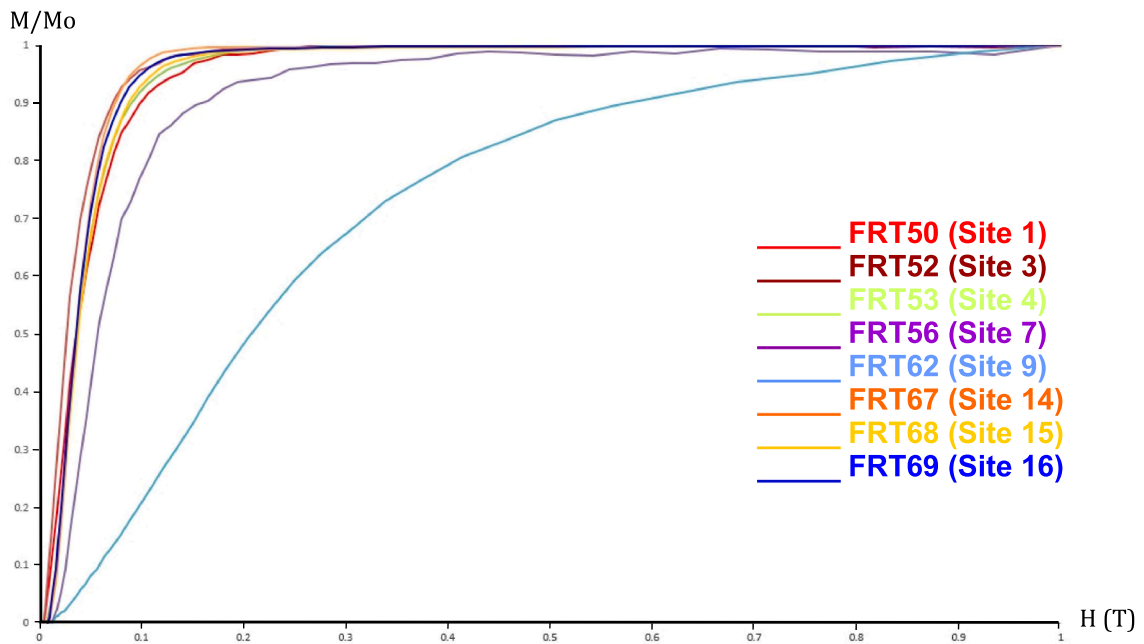


Fig. 6. Examples of IRM acquisition curves (normalized intensities versus magnetic field). Sample FRT62 represents the siltstone while other samples are from the Huanchaca sills.

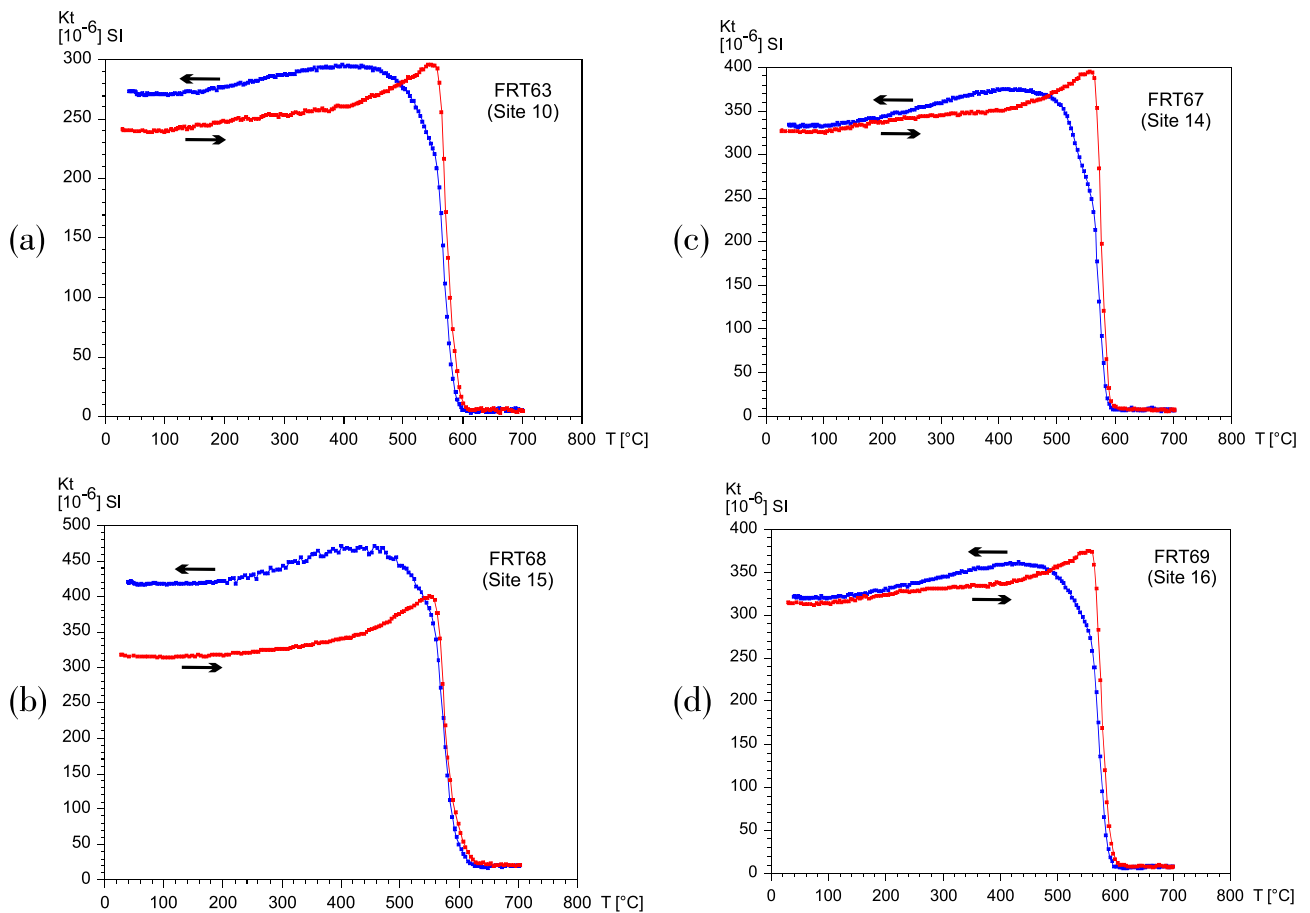
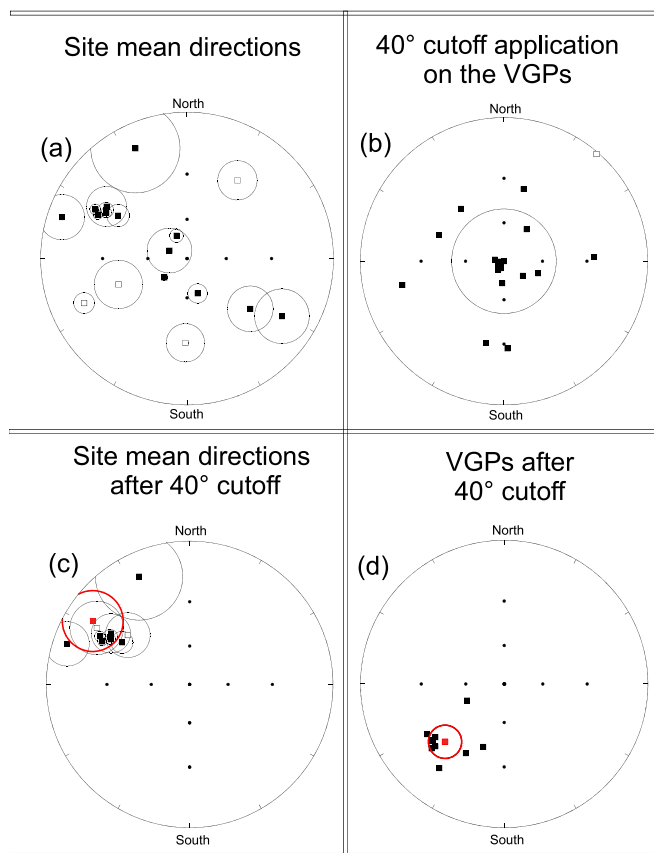


Fig. 7. Typical thermomagnetic curves showing variation in magnetic susceptibility  $K(SI)$  versus temperature. Curves were corrected for furnace effects. Heating in red and cooling in blue. (For interpretation of the references to color in this figure legend, the reader is referred to the web version of this article.)



**Fig. 8.** (a) Site mean directions for the Huanchaca sills and the siltstone. (b) 40° cutoff application on the respective VGP. (c) Site mean directions after 40° cutoff with its mean direction and respective confidence circle in red ( $\alpha_{95} = 14.5^\circ$ ). (d) VGPs after 40° cutoff with the HU pole and its respective confidence circle in red ( $\alpha_{95} = 9.9^\circ$ ). (For interpretation of the references to color in this figure legend, the reader is referred to the web version of this article.)

However, the fact that the investigated sedimentary rocks present directions similar to the Huanchaca sills component implies that both rock units acquired their magnetizations at the same time. The doubt is if the HU component represents a primary magnetization or a later overprint. Evidence in favor of the first hypothesis is that paleomagnetic analysis of the stratigraphically lower Fortuna Formation (Aguapeí Group), collected some 80–100 km away from Huanchaca sills yielded very different directions ( $D_m = 339.0^\circ$ ,  $I_m = -56.7^\circ$ ,  $N = 18$ ,  $\alpha_{95} = 7.3$ ,  $k = 24.0$ ) (D'Agrella-Filho et al., 2008). This implies that no regional remagnetization event affected all these rocks, and that probably the Huanchaca ChRM direction was acquired during sills intrusion.

- (5) The Huanchaca Suite is located on the Paraguá Terrain, between the Aguapeí and Sunsás mobile belts. The sills cut nearly horizontal sedimentary rocks from the Vale da Promissão Formation with no evidence that they were affected by later tectonic or metamorphic events (Teixeira et al., 2015, 2019; Lima et al., 2019);
- (6) Both polarities were registered, if magnetic directions from sites 5 (FRT54) and 20 (FRT73) were acquired during a reversal of the geomagnetic field, as we interpret. However, visually the normal and reversed directions are not anti-parallel, which does not pass this criterion according to Meert et al. (2020).
- (7) The Huanchaca pole is not similar to any younger pole from the Amazonian Craton.

In summary, the sills, magnetization was most probably acquired

during their intrusions and the Huanchaca pole can be considered as a robust paleomagnetic pole, classified with  $R = 5$ , according to the R-score of Meert et al. (2020).

## 6.2. Testing the Umkondia megacontinent

The Stenian (1200–1000 Ma) is the geological period where the Rodinia supercontinent was being formed (Li et al., 2008). According to these authors, Baltica, Amazonia/West Africa, Congo/São Francisco and Kalahari were drifting towards Laurentia, and collided along the Grenville orogenesis at ca. 1000 Ma. At ca. 1100 Ma, large igneous provinces (LIP) are described for most of these continental blocks: the 1109–1084 Ma large tectonomagmatic event known as the Keweenaw Mid-continental rift in Laurentia (Green et al., 1987; Swanson-Hysell et al., 2019); the 1110 Ma Rincón del Tigre-Huanchaca LIP in the Amazonian Craton (Teixeira et al., 2015; Reis et al., 2022); the 1110 Ma Huila-Epembe dykes and related mafic rocks in the Congo Craton (Salminen et al., 2018); and the 1110 Ma Umkondo LIP in the Kalahari Craton (Swanson-Hysell et al., 2015). Also, the Bundelkhand Craton (northwest India) was intruded by the  $1113 \pm 3$  Ma ENE-WSW Mahoba dykes (Pradhan et al., 2012).

In the last decade, paleomagnetic reconstructions for most of these 1110 Ma rocks have allowed paleomagnetic reconstructions to constrain the relative position of these cratonic blocks at this time (e.g., Swanson-Hysell et al., 2015; Salminen et al., 2018; Choudhary et al., 2019). Salminen et al. (2018) proposed a reconstruction at 1100 Ma where Kalahari was rotated clockwise relative to Congo-São Francisco (CSF). In their reconstruction, it is proposed that a common magmatic source originated the Huila-Epembe dykes in CSF and the Umkondo dykes in Kalahari, which was situated in the (present) northwestern Kalahari Craton. Salminen et al. (2018) also proposed that Kalahari (attached to CSF) collided later with Laurentia to form Rodinia as already previously suggested (e.g., Li et al., 2008; Loewy et al., 2011; de Kock et al., 2014; Swanson-Hysell et al., 2015).

Choudhary et al. (2019) included in the configuration of Salminen et al. (2018) the Amazonia/West Africa and India cratonic blocks arguing that the ca. 1110 Ma Rincón del Tigre-Huanchaca intrusions and Mahoba dykes originated from the same Umkondo plume center situated at northwestern Kalahari Craton. Their hypothetical supercraton, named by them as Umkondia (formed by Amazonia/West Africa, CSF, Kalahari and India), is considered as a megacontinent that later collided with Laurentia (linked to other cratonic blocks) forming Rodinia at ca. 1000–900 Ma (Wang et al., 2021). Lacking evidence of a collision, Choudhary et al. (2019) suggested that the Amazonia-West Africa block amalgamated to the Congo-CSF through a transcurrent fault-slip developed between 1380 and 1110 Ma.

The 1110 Ma Huanchaca pole from this study represents a great opportunity to test the reconstruction of the Umkondia megacontinent, which is shown in Fig. 11. Euler rotation poles used for each cratonic block in this reconstruction are presented in Table 2. Also shown are selected ~ 1100 Ma paleomagnetic poles for each block. Unfortunately, no 1100 Ma pole is presently available for West Africa. So, we considered the position of Amazonia and West Africa as in the West Gondwana configuration, although other different links have also been proposed for the Paleoproterozoic at ca. 1900–2000 Ma (e.g., Johansson, 2009; Bispo-Santos et al., 2014a,b; Antonio et al., 2021, and references therein). Congo is represented by the Huila-Epembe pole (Salminen et al., 2018), Kalahari by the Post-Gupera dykes (Evans, 2021) and Umkondo grand mean (Swanson-Hysell et al., 2015) poles and India by the Mahoba dykes pole (Pradhan et al., 2012). Finally, Amazonia is represented by the Huanchaca pole from this study. These poles cluster around the North Pole after they were rotated using the respective Euler poles calculated for each cratonic block used in the reconstruction of Fig. 11, supporting the Umkondia megacontinent, if we consider the uncertainties associated to the paleomagnetic poles and their ages.

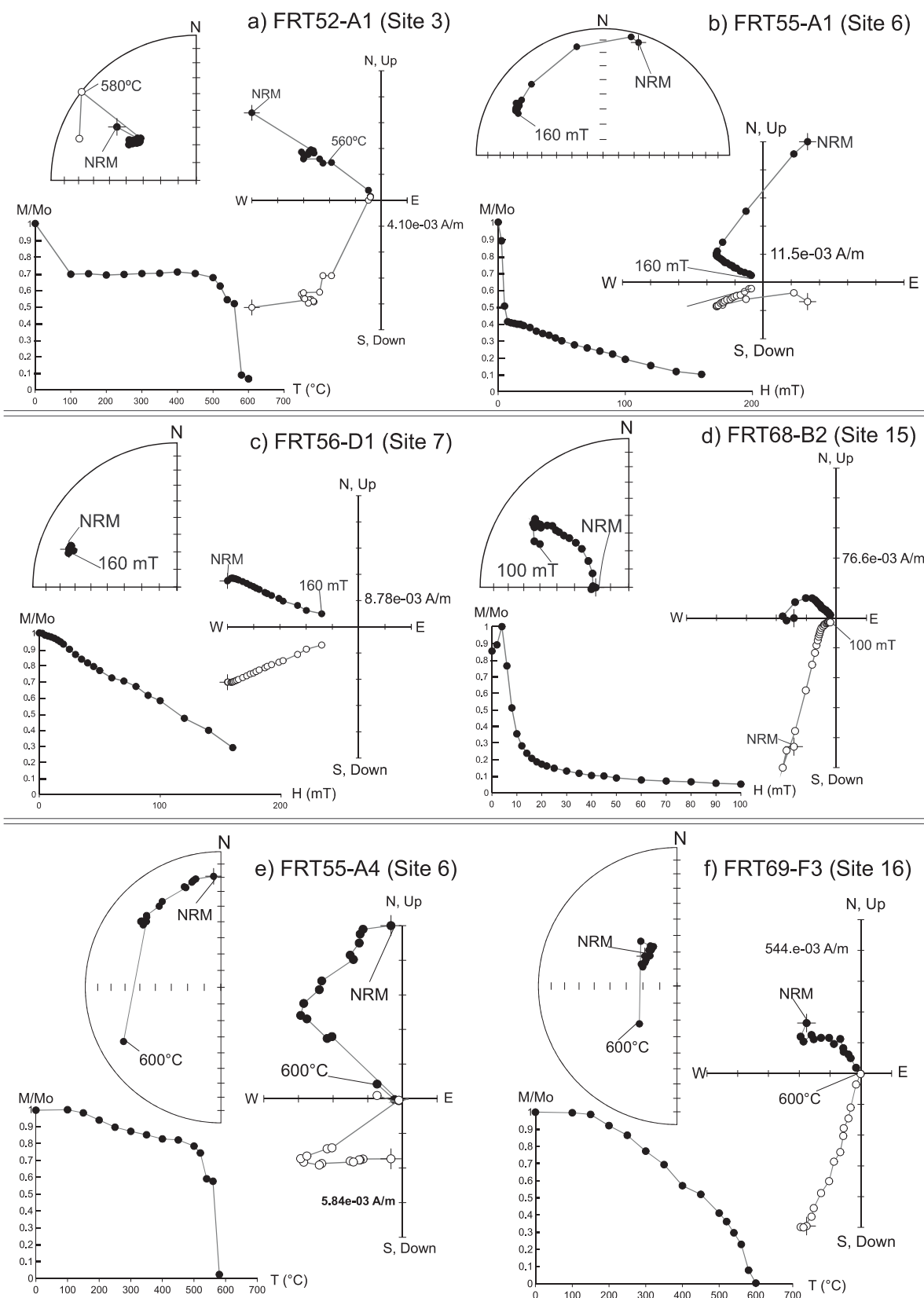


**Fig. 9.** Examples of AF and thermal demagnetization for samples from four sills sites. The figure shows stereographic projections (solid (open) symbols represent positive (negative) inclinations), normalized magnetization intensity curves (M/Mo versus alternating field (H) or temperature (T)) and orthogonal projections (solid (open) symbols represent horizontal (vertical) projections) for each sample.

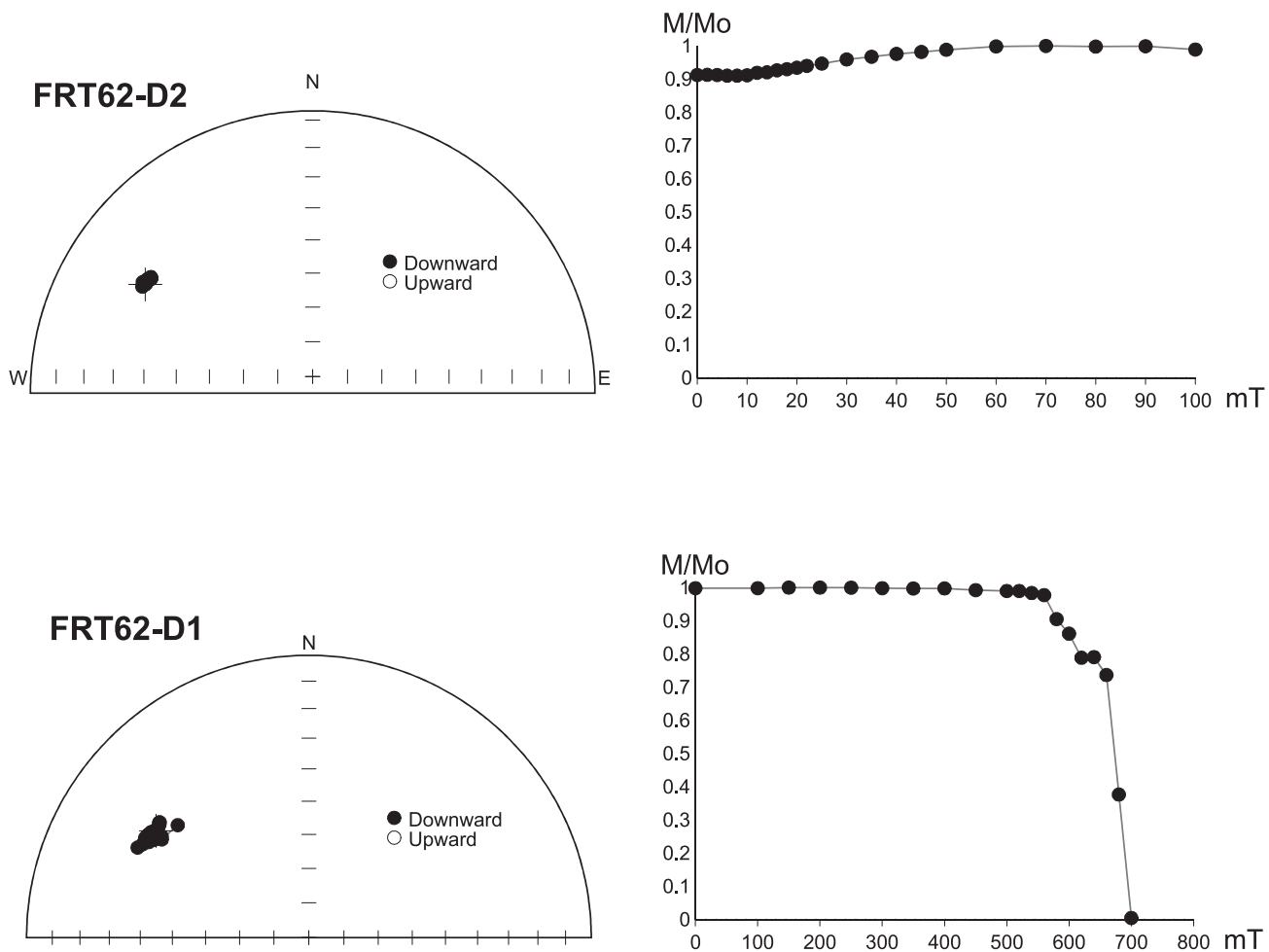


**Fig. 10.** Examples of AF and thermal demagnetization for two samples from siltstones (Vale do Promissão Formation). The figure shows stereographic projections and normalized magnetization intensity curves ( $M/M_o$  versus alternating field ( $H$ ) or temperature ( $T$ )) for each sample.

### 6.3. The role of Laurentia, Baltica and Umkondia in Rodinia agglutination

Very similar to Gondwana amalgamation, the Rodinia supercontinent was formed by different geodynamic events, occurred in a series of asymmetric subduction and collisional processes during the Stenian Period (Martin et al., 2020). Most probably, the Kalahari, Amazonian, Baltic and Laurentian cratons participated of its great mass, whose collisions generated mobile belts that record well the tectonic events of that period (Martin et al., 2020; Quadros et al., 2021). Orogens like the Sunsás, Grenville and Sveconorwegian are reflections of the collisional process involving Amazonia, Laurentia and Baltica at around 1000 Ma which are considered as being within the central portion of Rodinia (Slagstad et al., 2019).

There is consensus in the literature that Amazonia collided with Laurentia to form Rodinia, and that they were linked along the Sunsás-Grenville orogenesis at ca. 1000–950 Ma ago (e.g., Li et al., 2008, Johansson, 2009, Martin et al., 2020; Johansson et al., 2022, and references therein). However, the dynamics involved during this collision have been intensively debated. An oblique collision of Amazonia along the Llanos orogeny in Texas at 1200 Ma, followed by transcurrent movement relative to Laurentia up to 1000 Ma when it collided with Baltica, received geological, geochronological and paleomagnetic support (e.g., Tohver et al., 2002, 2004a, 2004b, D'Agrella-Filho et al., 2008, Ibañez-Mejía et al., 2011; Ibañez-Mejía, 2020). However, the 1100 Ma Huanchaca pole determined here doesn't support this interpretation (see below).

An alternative model proposed a collision of Amazonia with Laurentia along the area formed by Labrador, western Scotland, Greenland, northwestern Ireland and the Rockall Plateau (the Labrador-Scotland-Greenland promontory (LSGP) of Dalziel, 1992, 1994). However, distinct Pb isotopic data from LSGP and the southwestern Amazonian Craton led Loewy et al. (2003) to reject a collision of Amazonia along this Grenvillian area. Alternatively, Loewy et al. (2003) suggest a collision of the southwestern Amazonia along the central and southern Appalachian Grenvillian area, based on similarities in both ages and isotopic signatures between these two areas.

Based on the arguments presented above and in the available ca. 1100 Ma paleomagnetic poles, Laurentia and Baltica were included in our reconstruction of Umkondia (Fig. 11), now redrawn in Fig. 12. In this figure, the position of Laurentia is the same as proposed by Salminen et al. (2018) in their reconstruction of this landmass relative to Kalahari and CSF. Northern Baltica is linked to northeastern Laurentia and northwestern Amazonia is linked to western Baltica in a position that is reminiscent of the SAMBA reconstruction of Johansson (2009). Euler rotation poles calculated for Laurentia and Baltica are presented in Table 2. Selected ca. 1110 Ma paleomagnetic poles for Baltica and Laurentia are also shown in Table 2. Baltica is represented by the SD pole obtained for the well-dated  $1122 \pm 7$  Ma Salla Diabase Dyke (Salminen et al., 2009). Six poles are from Laurentia, extracted from Evans (2021): the  $1105 \pm 2$  Ma Lower Mamaince Point volcanic-R2 pole (L1); the  $1105 \pm 2$  Ma Upper Osler volcanic-R pole (L2); the  $1107 \pm 3$  Ma Middle Osler volcanic-R pole (L3); the  $1108 \pm 3$  Ma Lowermost Mamaince Point volcanics-R1 pole (L4); the  $1108 \pm 3$  Ma Lower Osler volcanic-R pole

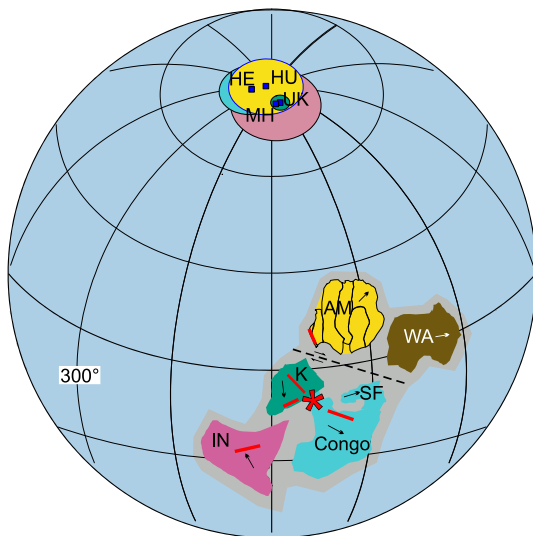


**Fig. 11.** Paleogeographic reconstruction of Umkondia (Amazonian Craton, West Africa, Congo, Kalahari and India) at 1100 Ma according to Choudhary et al. (2019). Euler rotation poles used for each craton in the reconstruction are presented in Table 2. The 1100 Ma paleomagnetic poles for each craton (after rotating them using the Euler pole of the corresponding craton) are also shown (Table 2). Paleomagnetic pole and respective craton are shown in the same color. AM - Amazonian Craton; WA - West Africa; K - Kalahari; SF - São Francisco Craton; IN - India. Paleomagnetic pole codes (HE, UK, MH, HU) are described in Table 2). Arrow in each craton represents the present north geographic direction. Red star represents the magmatic plume center that gave origin to the Huila-Epembe dyke swarm in Congo Craton, the Umkondo LIP in Kalahari, the Huanchaca LIP in Amazonia and the Mahoba dykes in India. (For interpretation of the references to color in this figure legend, the reader is referred to the web version of this article.)

(L5) and the 1111 ± 4 Ma Mean Nipigon sills and dykes pole (L6) (Table 2).

In the reconstruction, it is suggested that Laurentia and Baltica were also linked to Umkondia at 1100 Ma. After 1100 Ma, Baltica broke-up from Laurentia and, together with the rest of the Umkondia

megacontinent, it rotated clockwise colliding again with Laurentia, Amazonia at the Apalachian area and Kalahari at the Texas region, as already suggested by other authors (e.g., Loewy et al., 2003, Li et al., 2008).

Johansson (2009) and Johansson et al. (2022) also proposed a similar model for the break-up of their SAMBA reconstruction in the Columbia supercontinent, although for them rupture of Baltica/Amazonia occurred at ca. 1260 Ma ago, associated to the magmatic activities represented by the Mackenzie dyke swarm in Laurentia and the Central Scandinavian Dolerite Group in Fennoscandia. In fact, the timing of Baltica break-away from Laurentia is still disputed (e.g., Cawood and Pisarevsky, 2017). These authors argue that rupture occurred after 1260 Ma, but not necessarily at this time. For example, Yakubchuk (2019) believes that the Columbia supercontinent was reorganized into Rodinia without significant continental breakup. For Yakubchuk (2019), Columbia broke-up due to several rifting episodes near 1180 Ma and Rodinia reassembled around 1100–1040 Ma. On the other hand, Cawood and Pisarevsky (2017) admit the break-up initiation occurred after 1100 Ma (with the formation of the Asgard sea), as also suggested here, based on the reconstruction of Fig. 12.

Although paleomagnetic data corroborate the reconstruction in Fig. 12, the Meso- to Neoproterozoic evolution of the northwestern Amazonian Craton with the development of the ca. 1000 Ma Putumayo orogeny (Ibañez-Mejía et al., 2011; Ibañez-Mejía, 2020) seems to prevent a direct connection of northwestern Amazonia with Baltica at 1100 Ma, as suggested in Fig. 12 (see also Cawood and Pisarevsky, 2017). Trying to circumvent this problem an alternative reconstruction for Umkondia relative to Baltica and Laurentia is presented in Fig. 13. As the longitude paleomagnetic ambiguity permit, the Umkondia megacontinent was rotated 30° clockwise around the north pole (Euler pole at 90°N) in this reconstruction. As in the reconstruction of Fig. 12, here we can also envisage a clockwise rotation of Umkondia after 1100 Ma until it collided with Laurentia along the Appalachians’ Grenville front. This new model permits that the Colombian–Oaxaquian fringing-arc system as idealized by Ibañez-Mejía et al. (2011) and Ibañez-Mejía (2020) be formed in the northwestern Amazonian Craton. Meanwhile, Baltica rotated clockwise colliding with the northern Amazonian Craton at ca. 1000 Ma forming the Svecovergian belt during the 1050–980 Ma Agder phase (Cawood and Pisarevsky, 2017). If we consider the SAMBA link in

**Table 2**

Selected ca. 1100 Ma paleomagnetic poles for Baltica, Laurentia, Amazonia, West Africa, Kalahari, Congo-São Francisco and India and respective Euler rotation poles.

CRATON / Geological unit	Code	Age Ma	PLat. (°N)	PLon. (°E)	A95 (°)	Rlat. (°N)	Rlong. (°E)	R	Ref.
<b>BALTICA</b> – Rotation pole: 39.53°N, 77.01°E (45.6°)									
Salla Diabase Dyke	SD	1122 ± 7	71.0	113.0	8.1	71.8	280.1	5	1
<b>LAURENTIA</b> – Rotation pole: 3.80°N, 143.6°E (41.46°)									
Lower Mamainse Point volcanic – R2	L1	1105 ± 2	37.5	205.2	4.5	67.6	164.7	7	2
Upper Osler volcanic-R	L2	1105 ± 2	42.5	201.6	3.7	67.9	149.6	7	2
Middle Osler volcanic-R	L3	1107 ± 3	42.7	211.3	8.2	74.3	159.5	6	2
Lowermost Mamainse Point volcanic s-R1	L4	1108 ± 3	49.5	227.0	5.3	86.5	128.8	7	2
Lower Osler volcanic-R	L5	1108 ± 3	40.9	218.6	4.8	77.7	178.9	6	2
Mean Nipigon sills and dykes	L6	1111 ± 4	47.2	217.8	4.0	80.3	148.1	5	2
<b>AMAZONIA</b> – Rotation pole: 48.49°N, 176.73°E (95.7°)									
Huanchaca sills	HU	1112 ± 2	21.7	240.5	15.3	74.8	1.2	5	3
<b>WEST AFRICA</b> – Rotation pole: 12.43°N, 194.21°E (101.74°)									
<b>CONGO</b> – Rotation pole: 13.81°N, 195.64°E (126.43°)									
Huila Epembe	HE	1110 ± 3; 1109 ± 10	-34.7	256.5	8.7	84.5	276.3	6	4
<b>SÃO FRANCISCO</b> – Rotation pole: 41.04°N, 174.22°E (117.58°)									
<b>INDIA</b> – Rotation pole: 52.56°N, 281.14°E (-100.26°)									
Mahoba dykes	MH	1113 ± 7	+38.7	229.5	12.4	84.0	10.0	4	5
<b>KALAHARI</b> – Rotation pole: 14.73°N, 196.54°E 169.56°)									
Post-Gupera dykes	PG	1105 ± 1	62.3	31.9	6.9	85.9	327.1	6	2
Umkondo mean	UK	1109 ± 1; 1112 ± 1	-64.0	222.1	2.6	84.1	22.3	5	6

Plat. – Pole latitude; Plong. – Pole longitude; A95 – radius of 95% confidence cone; Rlat – rotated pole latitude; Rlong – rotated pole longitude; Reference: 1 - Salminen et al. (2009); 2 - Evans (2021); 3 - This work; 4 - Salminen et al. (2018); 5 - Pradhan et al. (2012); 6 - Swanson-Hysell et al. (2015). For reconstruction of Fig. 13, Umkondia and respective poles (Rlat., Rlong.) were rotated 30° clockwise around the Euler pole at (90°N, 0°E).

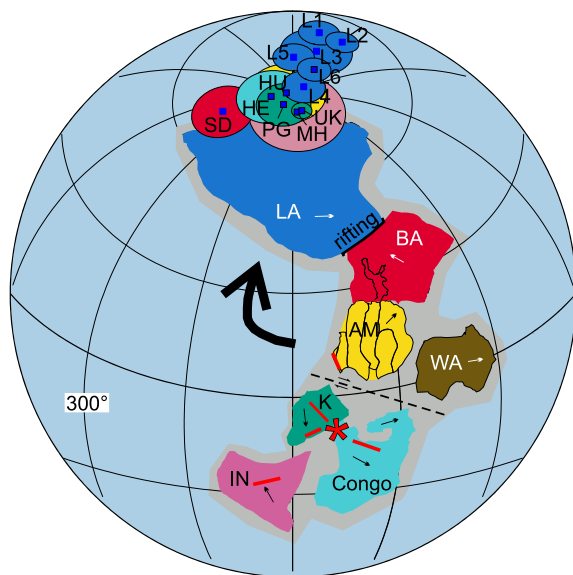


**Fig. 12.** Paleogeographic reconstruction of Umkondia, Baltica and Laurentia at 1100 Ma in the Rodinia supercontinent. Euler rotation poles used for each craton in the reconstruction are presented in Table 2. The 1100 Ma paleomagnetic poles for each craton (after rotating them using the Euler pole of the corresponding craton) are also shown (Table 2). Paleomagnetic pole and respective craton are shown in the same color. LA - Laurentia; BA - Baltica; AM - Amazonian Craton; WA - West Africa; K - Kalahari; SF - São Francisco Craton; IN - India. Paleomagnetic pole codes (L1, L2, L3, L4, L5, L6, SD, HE, UK, MH, HU, PG) are described in Table 2. Arrow in each craton represents the present north geographic direction. Red star represents the magmatic plume center that gave origin to the Huila-Epembe dyke swarm in Congo Craton, the Umkondo LIP in Kalahari, the Huanchaca LIP in Amazonia and the Mahoba dykes in India. See text for details. Greater arrow indicates the Umkondia movement after 1100 Ma. (For interpretation of the references to color in this figure legend, the reader is referred to the web version of this article.)

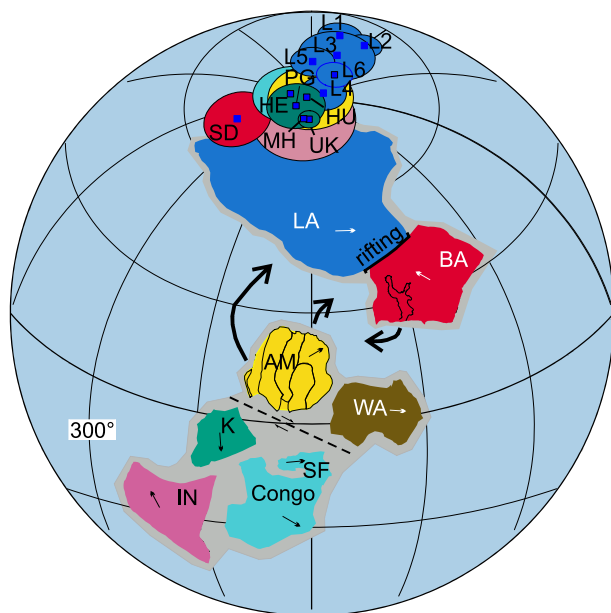


**Fig. 13.** The same as in Fig. 12 with Umkondia and their respective paleomagnetic poles rotated 30° clockwise around North geographic Pole (Euler pole at 90°N, 0°E). Details are described in the legend of Fig. 12. See text for details. Greater arrows indicate the Umkondia and Baltica movements after 1100 Ma.

the Columbia supercontinent as correct (Johansson, 2009), the time at

which the Amazonian Craton separated from Baltica is yet undefined, although a possibility is that this occurred at ca. 1400 Ma as suggested by the 1440–1420 Ma Amazonian paleomagnetic data (e.g., D'Agrella-Filho et al., 2016, 2021). Another possibility is that Amazonia/West Africa drifted as an independent continental block in the Paleoproterozoic and was never part of Columbia (Pisarevsky et al., 2014, Cawood and Pisarevsky, 2017).

Another point that merits discussion is the time of collision between the Arequipa/Antofala Block (AAB) located in the proto-Andean margin of Amazonia (Ramos, 1988) with the Amazonian Craton. The geological evolution of AAB began in the Paleoproterozoic (2000–1900 Ma) in its northern part, and it was affected by magmatism and/or deformation at three periods: ca. 1500–1400 Ma, ca. 1200–1000 Ma and ca. 500–440 Ma (e.g., Loewy et al., 2004). The similar 1200–1000 Ma Sunsás metamorphic episode led some authors to suggest an accretion of the AAB to the Amazonian Craton during the Sunsás orogeny (e.g., Dalziel, 1994, Boger et al., 2005 and references therein), while others suggest a later collision, during Cambrian to Ordovician times (Ramos, 1988, Ramos et al., 1993, Coira et al., 1982). A late Mesoproterozoic collision would imply that the AAB had to be included between Amazonia and Laurentia at ca. 1000 Ma ago. However, comparing Pb isotopic data from AAB with those from the Amazonian, Laurentian and Kalahari cratons, Loewy et al. (2003) proposed a model where AAB was part of the Kalahari craton due to their greater isotopic affinities. Then, both, Amazonia and Kalahari/AAB, collided with Laurentia along the Appalachians and Texas areas, respectively. When Kalahari broke-up from Laurentia it left AAB behind, which rotated and amalgamated with Amazonia at ca. 500 Ma (Loewy et al., 2003).

## 7. Final remarks

Paleomagnetic analysis was performed on rocks from the 1112 Ma (U–Pb, baddeleyite) mafic sills from the Huanchaca Intrusive Suite, SW Amazonian Craton (western Mato Grosso State, Brazil). AF and thermal treatments revealed northwestern characteristic remanent magnetization (ChRM) directions with low positive/negative inclinations, carried by stable PSD magnetite. A mean direction was calculated ( $D_m = 303.2^\circ$ ,  $I_m = 12.2^\circ$ ,  $N = 10$ ,  $\alpha_{95} = 14.5^\circ$ ,  $k = 12.0$ ), which yielded the paleomagnetic pole (HU) located at  $30.1^\circ\text{N}$ ;  $225.7^\circ\text{E}$ , ( $A_{95} = 9.9^\circ$ ), classified with a reliability factor  $R = 5$ . The Huanchaca paleopole favors the existence of the Umkondia (Kalahari/CSF/Amazonia/West Africa/India) megacontinent at 1100 Ma, which latter collided with Laurentia forming the Rodinia supercontinent around 1000–900 Ma. Compared to Laurentia and Baltica, two paleogeographies at 1100 Ma are possible: (1) Northeastern Laurentia was linked to northern Baltica and northwestern Amazonia was linked to southwestern Baltica as in the SAMBA configuration of Columbia. Baltica (linked to Umkondia) broke-up from Laurentia and rotated clockwise up to its collision with Laurentia to form Rodinia; (2) Laurentia was linked to Baltica, but Amazonia (in the Umkondia configuration) was separated from Baltica. After 1100 Ma, Umkondia executed a clockwise rotation colliding with Laurentia. At the same time, Baltica broke-up from Laurentia and also rotated clockwise colliding with Amazonia. The second model is preferred since it can explain the development of the 1150–1000 Ma Colombian-Oaxaquian fringing-arc system (Ibañez-Mejía et al., 2011; Ibañez-Mejía, 2020) and the Svecoferric 1050–980 Ma belt after the Agder ocean opening (Cawood and Pisarevsky, 2017).

## CRedit authorship contribution statement

**Franklin Bispo-Santos:** Writing – original draft, Writing – reviewing and editing, Formal analysis. **Manoel S. D'Agrella-Filho:** Writing – reviewing and editing, Project administration. **Renato P. de Almeida:** Supervision, Validation. **Amarildo S. Ruiz:** Investigation, Conceptualization. **Oscar A.L. Patroni:** Formal analysis. **Julia Massucato Silva:** Formal analysis.

## Declaration of Competing Interest

The authors declare the following financial interests/personal relationships which may be considered as potential competing interests: Manoel D'Agrella-Filho reports financial support was provided by FAPESP (State of Sao Paulo Research Foundation). Manoel D'Agrella-Filho reports financial support was provided by National Council for Scientific and Technological Development (CNPq). Franklin Bispo-Santos reports financial support was provided by Coordination for the Improvement of Higher Education Personnel (CAPES).

## Data availability

Data will be made available on request.

## Acknowledgments

We thank the financial support by FAPESP (grants 2016/13689-5 and 2021/01976-8). F. Bispo-Santos thanks CAPES for the research fellowship by Geosciences Institute of University of São Paulo (IGc-USP). M.S. D'Agrella-Filho thanks CNPq for the Research fellowship (grant 308330/2021-8). We also thank the Federal University of Mato Grosso (UFMT) for its help in field work logistics and the USPMag Laboratory from the IAG and the CORE laboratory in Oceanographic Institute of the University of São Paulo (IO-USP) which made the magnetic experimental work possible. We also thank to Michiel de Kock, to anonymous reviewer, and the editor Sergei Pisarevsky for their constructive reviews that greatly improved the manuscript.

## References

- Antonio, P.Y.J., D'Agrella-Filho, M.S., Nédélec, A., Poujol, M., Sanchez, C., Dantas, E.L., Dall'Agnol, R., Teixeira, M.F.B., Proietti, A., Martínez Dopico, C.I., Oliveira, D.C., Silva, F.F., Marangoanha, B., Trindade, R.I.F., 2021. New constraints for paleogeographic reconstructions at ca. 1.88 Ga from geochronology and paleomagnetism of the Carajás dyke swarm (eastern Amazonia). *Precambrian Res.* 353, 106039.
- Bettencourt, J.S., Leite Jr., W., Payolla, B., Ruiz, A.S., Matos, R.S., Tosdal, R.M., 2010. The Rondonian-San Ignacio Province in the SW Amazonian Craton: an overview. *J. S. Am. Earth Sci.* 29, 28–46.
- Bispo-Santos, F., D'Agrella-Filho, M.S., Janikian, L., Reis, N.J., Reis, M.A.A.A., Trindade, R.I.F., 2014a. Towards Columbia: Paleomagnetism of 1980–1960 Ma Surumu volcanic rocks, Northern Amazonian Craton. *Precamb. Res.* 244, 123–138.
- Bispo-Santos, F., D'Agrella-Filho, M.S., Trindade, R.I.F., Janikian, L., Reis, N.J., 2014b. Was there SAMBA in Columbia? Paleomagnetic evidence from 1790 Ma Avanavero mafic sills (Northern Amazonian craton). *Precamb. Res.* 244, 139–155.
- Boger, S.D., Raetz, M., Giles, D., Etchart, E., Fanning, C.M., 2005. U-Pb age data from Sunas region of Eastern Bolivia, evidence for the allochthonous origin of the Paragua Block. *Precamb. Res.* 139, 121–146.
- Brito Neves, B.B., Cordani, U.G., 1991. Tectonic Evolution of South America during the Late Proterozoic. *Precamb. Res.* 53, 23–40. [https://doi.org/10.1016/0301-9268\(91\)90004-T](https://doi.org/10.1016/0301-9268(91)90004-T).
- Cawood, P.A., Pisarevsky, S.A., 2017. Laurentia-Baltica-Azonian relations during Rodinia assembly. *Precamb. Res.* 292, 386–397.
- Cawood, A., Strachan, R.A., Pisarevsky, S.A., Gladkochub, D.P., Murphy, J.B., 2016. Linking collisional and accretionary orogens during Rodinia assembly and breakup: Implication for models of supercontinent cycles. *Earth Planet. Sci. Lett.* 449, 118–126.
- Choudhary, B.R., Ernest, R.E., Xu, Y.-G., Evans, D.A.D., de Kock, M.O., Meert, J.G., Ruiz, A.S., Lima, G.A., 2019. Geochemical characterization of a reconstructed 1110 Ma Large Igneous Province. *Precambrian Res.* 332, 1–22. <https://doi.org/10.1016/j.precamres.2019.105382>.
- Coira, B., Davidson, J., Mpodozis, C., Ramos, V.A., 1982. Tectonic and magmatic evolution of the Andes of northern Argentina and Chile. *Earth Sci. Rev.* 18 (3), 303–332. [https://doi.org/10.1016/0012-8252\(82\)90042-3](https://doi.org/10.1016/0012-8252(82)90042-3).
- Cordani, U. G., Fraga, L. M., Reis, N., Tassinari, C. C. G., Brito-Neves, B. B., 2010. On the origin and tectonic significance of the intra-plate events of Grenvillian-type age in South America: A discussion. *J. South American Earth Sci.* 29, 143–159.
- Cordani, U.G., Teixeira, W., 2007. Proterozoic accretionary belts in the Amazonian Craton. *Geol. Soc. Am. Mem.* 200, 297–320.
- D'Agrella-Filho, M.S., Antonio, P.Y.J., Trindade, R.I.F., Teixeira, W., Bispo-Santos, F., 2021. The Precambrian drift history and paleogeography of Amazonia. In: Pesonen, L., Elming, S.-Å., Evans, D.A.D., Veikkolainen, T. (Org.). *Ancient Supercontinents and the Paleogeography of Earth*. Elsevier, book, Chapter 6, 207–241.
- D'Agrella-Filho, M.S., Tohver, E., Santos, J.O.S., Elming, S.-Å., Trindade, R.I.F., Pacca, I. G., Geraldés, M.C., 2008. Paleomagnetism of the 1.15 Ga Aguapeí Group (SW Amazon Craton): Evidence for the tectonic evolution of Rodinia. *Earth Planetary Sci. Lett.* 267, 188–199. <https://doi.org/10.1016/j.epsl.2007.11.030>.
- D'Agrella-Filho, M.S., Trindade, R.I.F., Elming, S.A., Teixeira, W., Yokoyama, E., Tohver, E., Geraldés, M.C., Pacca, I.L.G., Barros, M.A.S., Ruiz, A.S., 2012. The 1420 Ma Indivaí Mafic Intrusion (SW Amazonian Craton): Paleomagnetic results and implications for the Columbia supercontinent. *Gondw. Res.* 22, 956–973.
- D'Agrella-Filho, M.S., Trindade, R.I.F., Queiroz, M.V.B., Meira, V.T., Janikian, L., Ruiz, A.S., Bispo-Santos, F., 2016. Reassessment of Aguapeí (Salto do Céu) paleomagnetic pole, Amazonian Craton and implications for Proterozoic supercontinents. *Precamb. Res.* 272, 1–17.
- Dalziel, I.W.D., 1992. On the organization of American plates in the Neoproterozoic and breakup of Laurentia. *GSA Today* 2, 240–241.
- Dalziel, I.W.D., 1994. Precambrian Scotland as a Laurentia-Gondwana link: Origin and significance of cratonic promontories. *Geology* 22 (7), 589–592.
- Day, R., Fuller, M., Schmidt, V.A., 1977. Hysteresis properties of titanomagnetites: Grain size and composition dependence. *Phys. Earth Planet. Interiors* 13, 260–267.
- de Kock, M.O., Ernst, R., Söderlund, U., Jourdan, F., Hofmann, A., Le Gall, B., Bertrand, H., Chisonga, B.C., Beukes, N., Rajesh, H.M., Moseki, L.M., Fuchs, R., 2014. Dykes of the 1.11 Ga Umkondo LIP, Southern Africa: Clues to a complex plumbing system. *Precambrian Res.* 249, 129–143.
- De Melo, R.P., De Oliveira, M.A.F., Goldfarb, R.J., Johnson, C.A., Marsh, E.E., de Oliveira, L.R., Morgan, L.E., 2022. Early neoproterozoic gold deposits of the Alto Guaporé province, Southwestern Amazon Craton, Western Brazil. *Economic Geology* 117(1), 127–163. [doi:10.5382/econgeo.4852](https://doi.org/10.5382/econgeo.4852).
- Deenen, M.H.L., Langereis, C.G., van Hinsbergen, D.J.J., Biggin, A.J., 2011. Geomagnetic secular variation and the statistics of palaeomagnetic directions. *Geophys. J. Interiors* 186, 509–520. <https://doi.org/10.1111/j.1365-246X.2011.05050.x>.
- Dunlop, D.J., 2002. Theory and application of the Day plot (Mrs/Ms versus Hcr/Hc) 1. Theoretical curves and tests using titanomagnetite data. *J. Geophys. Res.* 107 <https://doi.org/10.1029/2001JB000486>.
- Dunlop, D.J., Ozdemir, O., 1997. *Rock Magnetism, Fundamentals and Frontiers*. Cambridge University Press, Cambridge, 573 p.
- Evans, D.A.D., 2013. Reconstructing pre-Pangean supercontinents. *Geol. Soc. Am. Bulletin*, 125: 1735–1751. Fisher, R. A., 1953. Dispersion on a Sphere. *Proc. R. Soc. Lond.* 217, 295–305.
- Evans, D.A.D., 2021. Meso-Neoproterozoic Rodinia supercycle. In: Pesonen, L.P., Salminen, J., Evans, D.A.D., Elming, S.-Å., Veikkolainen, T. (Eds.), *Ancient Supercontinents and the Paleogeography of the Earth*. Elsevier, book, Chapter 17, 549–576.
- Eyster, A., Weiss, B.P., Karlstrom, K., Macdonald, F.A., 2019. Paleomagnetism of the Chuar Group and evaluation of the late Tonian Laurentian apparent polar wander path with implications for the breakup and Rodinia. *GSA Bull.* 132 (3/4), 710–738. <https://doi.org/10.1130/B32012.1>.
- Fisher, R.A., 1953. Dispersion on a sphere. *Proc. R. Soc. Lond.* 217, 295–305.
- Geraldés, M.C., Nogueira, C., Vargas-Mattos, G., Matos, R., Teixeira, W., Valencia, V., Ruiz, J., 2014. U-Pb detrital zircon ages from the Aguapeí Group (Brazil): Implications for the geological evolution of the SW border of the Amazonian Craton. *Precamb. Res.* 244 (1), 306–316.
- Green, J. C., Bornhorst, T. J., Chandler, V. W., Mudrey Jr, M. G., Meyers, P. E., Pesonen, L., Wilband, J. T., 1987. Keweenaw dykes of the Lake Superior region: evidence for evolution of the Middle Proterozoic Midcontinent Rift of North America. In H. C. Halls, W. Fahrig (Eds.), *Mafic Dyke Swarms*. Geological Association of Canada, Special Paper, 34, 289–302.
- Ibañez-Mejía, M., Ruiz, J., Valencia, V.A., Cardona, A., Gehrels, G.E., Mora, A.R., 2011. The Putumayo Orogen of Amazonia and its implications for Rodinia reconstructions: New U-Pb geochronological insights into the Proterozoic tectonic evolution of northwestern South America. *Precamb. Res.* 191 (1–2), 58–77. <https://doi.org/10.1016/j.precamres.2011.09.005>.
- Ibañez-Mejía, M., 2020. The Putumayo Orogen of Amazonia: A synthesis. In: Gómez, J. & Mateus-Zabala, D. (editors), *The Geology of Colombia, Volume 1: Proterozoic – Paleozoic*. Servicio Geológico Colombiano, Publicaciones Geológicas Especiales, 35, p. 101–131. Bogotá. 10.32685/pub.es.35.2019.06.
- Jing, X., Yang, Z., Evans, D.A.D., Tong, Y., Xu, Y., Wang, H., 2020. A pan-latitude Rodinia in the Tonian true polar wander frame. *Earth Planet. Sci. Lett.* 530, 115880 <https://doi.org/10.1016/j.epsl.2019.115880>.
- Jing, X., Evans, D.A.D., Yang, Z., Tong, Y., Xu, Y., Wang, H., 2021. Inverted South China: A novel configuration for Rodinia and its breakup. *Geology* 49, 463–467. <https://doi.org/10.1130/G47807.1>.
- Johansson, A., 2009. Baltica, Amazonia and the SAMBA connection—1000 million years of neighbourhood during the Proterozoic? *Precamb. Res.* 175, 221–234. <https://doi.org/10.1016/j.precamres.2009.09.011>.
- Johansson, A., 2014. From Rodinia to Gondwana with the 'SAMBA' model – a distant view from Baltica towards Amazonia and beyond. *Precamb. Res.* 244, 226–235.
- Johansson, A., Bingen, B., Huhma, H., Waigant, T., Vestergaard, R., Soesoo, A., Skridlaite, G., Krzeminska, E., Shumlyansky, L., Holland, M.E., Holm-Denoma, C., Teixeira, W., Faleiros, F.M., Ribeiro, B.V., Jacobs, J., Wang, C., Thomas, R.J., Macey, P.H., Kirkland, C.L., Hartnady, M.I.H., Eglinton, B.M., Puetz, S.J., Condie, K. C., 2022. A geochronological review of magmatism along the external margin of Columbia and in the Grenville-age orogens forming the core of Rodinia. *Precamb. Res.* 371, 106463 <https://doi.org/10.1016/j.precamres.2021.106463>.
- Kirschvink, J.L., 1980. The least-squares line and plane and the analysis of palaeomagnetic data. *Geophys. J. Int.* 62 (3), 699–718.
- Lacerda-Filho, J. V., Abreu Filho, W., Valente, C. R., Oliveira, C. C., Albuquerque, M. C., 2004. *Geologia e Recursos Minerais do Estado do Mato Grosso*. Texto explicativo dos mapas geológico e de recursos minerais do Estado do Mato Grosso, Escala 1: 1.000.000, Convênio CPRM e SICME-MT, 235 p.

- Ledru, P., Johan, V., Milési, J.P., Tegye, M., 1994. Markers of the last stages of the paleoproterozoic collision: evidence for a 2 Ga continent involving circum- South Atlantic provinces. *Precamb. Res.* 69, 169–191.
- Leite, J.A.D., Saes, G.S., 2003. Geocronologia Pb/Pb de zircões detríticos e análise estratigráfica das coberturas sedimentares Proterozóicas do sudeste do Craton Amazônico. *Revista do Instituto de Geociências da USP* 3, 113–127.
- Li, Z.X., Bogdanova, S.V., Collins, A.S., Davidson, A., De Waele, B., Ernst, R.E., Fitzsimons, I.C.W., Fuck, R.A., Gladkochub, D.P., Jacobs, J., Karlstrom, K.E., Lu, S., Natapov, L.M., Pease, V., Pisarevsky, S.A., Thrane, K., Vernikovsky, V., 2008. Assembly, configuration, and break-up history of Rodinia: a synthesis. *Precamb. Res.* 160, 179–210.
- Lima, G.A., Sousa, M.Z.A., Ruiz, A.S., D'Agrella-Filho, M.S., Vasconcelos, P., 2012. Sills máficos da Suíte Intrusiva Huanchaca - SW do Cráton Amazônico: registro de magmatismo fissural relacionado à ruptura do Supercontinente Rodínia. *Revista Brasileira de Geociências* 42 (1), 111–129.
- Lima, G.A., Macambira, J.B., Sousa, M.Z.A., Ruiz, A.S., D'Agrella-Filho, M.S., 2019. Fissural mafic magmatism on southwestern Amazonian Craton: Petrogenesis and 40Ar-39Ar geochronology. *J. S. Am. Earth Sci.* 93, 214–231.
- Litherland, M., Annells, R.N., Darbyshire, D.P.F., Fletcher, C.J.N., Hawkins, M.P., Klinck, B.A., Mitchell, W.L., O'Connor, E.A., Pitfield, P.E.J., Power, G., Webb, B.C., 1989. The Proterozoic of Eastern Bolivia and its relationship to the Andean mobile belt. *Precamb. Res.* 43, 157–174.
- Loewy, S.L., Connelly, J.N., Dalziel, I.W.D., 2004. An orphaned basement block: The Arequipa-Antofalla Basement of the central Andean margin of South America. *GSA Bull.* 116 (1/2), 171–187. <https://doi.org/10.1130/B25226.1>.
- Loewy, S.L., Dalziel, I.W.D., Pisarevsky, S., Connelly, J.N., Tait, J., Hanson, R.E., Bullen, D., 2011. Coats Land crustal block, East Antarctica: A tectonic tracer for Laurentia? *Geology* 39, 859–862. <https://doi.org/10.1130/G32029.1>.
- Loewy, S.L., Connelly, J.N., Dalziel, I.W.D., Gower, C.F., 2003. Eastern Laurentia in Rodinia: Constraints from whole-rock Pb and U-Pb geochronology. In: *Sircombe, K. N., McElhinny, M.W., eds. Orogenic belts, regional and global tectonics: A memorial volume to Chris McAulay Powell. Tectonophysics* 375, 169–197.
- Martin, E.L., Spencer, C.J., Collins, W.J., Thomas, R.J., Macey, P.H., Roberts, N.M.W., 2020. The core of Rodinia formed by the juxtaposition of opposed retreating and advancing accretionary orogens. *Earth Sci. Rev.* 211, 103413 <https://doi.org/10.1016/j.earscirev.2020.103413>.
- McMenamin, M.A.S., McMenamin, D.L., 1990. *The Emergence of Animals: The Cambrian Breakthrough*. Columbia University Press, New York. 217 pp.
- Meert, J.G., Pivarunas, A.F., Evans, D.A.D., Pisarevsky, S.A., Pesonen, L.J., Li, Z.X., Elming, S.A., Miller, S.R., Zhang, S., Salminen, J.M., 2020. The magnificent seven: A proposal for modest revision of the Van der Voo (1990) quality index. *Tectonophysics* 790, 228549. <https://doi.org/10.1016/j.tecto.2020.228549>.
- Nadeau, S., Chen, W., Reece, J., Lachhman, D., Ault, R., Faraco, M.T.L., Fraga, L.M., Reis, N.J., Bettiolo, L.M., 2013. Guyana: The lost hadean crust of South America? *Braz. J. Geol.* 43 (4), 601–606.
- Pisarevsky, S.A., Elming, S.-Å., Pesonen, L.J., Li, Z.-X., 2014. Mesoproterozoic paleogeography: supercontinent and beyond. *Precamb. Res.* 244, 207–225.
- Pradhan, V.R., Meert, J.G., Pandit, M.K., Kamenov, G., Mondal, M.E.A., 2012. Paleomagnetic and geochronological studies of the mafic dyke swarms of Bundelkhand craton, central India: Implications for the tectonic evolution and paleogeographic reconstructions. *Precamb. Res.* 198–199, 51–76. <https://doi.org/10.1016/j.precamres.2011.11.011>.
- Quadros, M.L.E.S., Giustina, M.E.S.D., Souza, V.S., Scandolaria, J.E., 2020. Geology, geochemistry and Sr-Nd isotopes of the Rio Branco suite, Nova Brasilândia belt in southwest of the Amazon craton: evidence of a Rodinia pre-assembly accretionary phase (ca. 1137 and 1106 Ma) during the evolution of the Nova Brasilândia orogeny. *Lithos* 372–373. [10.1016/j.lithos.2020.105651](https://doi.org/10.1016/j.lithos.2020.105651).
- Quadros, M.L.E.S., Giustina, M.E.S.D., Rodrigues, J.B., Souza, V.S., 2021. Geology and LA-ICP-MS U-Pb geochronology of the Nova Brasilândia belt, SW Amazonian Craton: New ages, re-evaluation of existing geochronological data, and implications for the evolution of the Sunsas orogeny. *J. S. Am. Earth Sci.* 109, 103220 <https://doi.org/10.1016/j.jsames.2021.103220>.
- Ramos, V.A., 1988. Tectonics of the Late Proterozoic - Early Paleozoic: a collisional history of Southern South America. *Episodes* 11 (3), 168–174.
- Ramos, V.A., Vujovich, G., Kay, S.M., and McDonough, M., 1993. La orogenesis de Grenville en las Sierras Pampeanas Occidentales: La Sierra de Pie de Palo y su integración al supercontinente Proterozoico: XII Congreso Geológico Argentino y II Congreso de Exploración de Hidrocarburos Actas, v. T. III, p. 343–357.
- Reis, N.J., Teixeira, W., D'Agrella-Filho, M.S., Bettencourt, R.E., Ernst, L.E., Goulart, L.E., 2022. Large Igneous Provinces of the Amazonian Craton and their Metallogenic Potential in Proterozoic Times. In: *Srivastava, R.K., Ernst, R.E., Buchan, K.L., De Cock, M. (eds.). Large Igneous Provinces and their Plumbing Systems. Geological Society of London, Special Publications*. 518, 493–529. doi: 10.1144/SP518-2021.
- Rizzotto, G.J., Hartmann, L.A., 2012. Geological and geochemical evolution of the Trincadeira Complex, a Mesoproterozoic ophiolite in the southwestern Amazon craton, Brazil. *Lithos* 148, 277–295.
- Roberts, A.P., Heslop, D., Zhao, X., Pike, C.R., 2014. Understanding fine magnetic particle systems through use of first-order reversal curve diagrams. *Rev. Geophys.* 52, 557–602. <https://doi.org/10.1002/2014RG000462>.
- Sadowski, G.R., Bettencourt, J.S., 1996. Mesoproterozoic tectonic correlations between eastern Laurentia and Western border of the Amazon Craton. *Precamb. Res.* 76, 213–227.
- Saes, G.S., Leite, J.A.D., 1993. Evolução tectono-sedimentar do Grupo Aguapeí. Proterozoico médio na porção meridional do Cráton Amazônico: Mato Grosso e oriente boliviano: *Revista Brasileira de Geociências* 23, 31–37.
- Salminen, J., Pesonen, L. J., Mertanen, S., Vuollo, J., Airo, M.-L., 2009. Palaeomagnetism of the Salla Diabase Dyke, northeastern Finland, and its implication for the Baltica-Laurentia entity during the Mesoproterozoic. In: *S. M. Reddy, R. Mazumder, D. A. D. Evans, A. S. Collins (Eds.), Palaeoproterozoic supercontinents and global evolution. Geological Society, special publication* 323, 199–217. [10.1144/SP323.9](https://doi.org/10.1144/SP323.9).
- Salminen, J., Hanson, R., Evans, D.A.D., Gong, Z., Larson, T., Walker, O., Gumsley, A., Söderlund, U., Ernst, R., 2018. Direct Mesoproterozoic connection of the Congo and Kalahari cratons in proto-Africa: Strange attractors across supercontinental cycles. *Geology* 46 (11), 1011–1014.
- Santos, J.O.S., Hartmann, L.A., Gaudette, H.E., Groves, D.I., McNaughton, N.J., Fletcher, I.R., 2000. A new understanding of the Provinces of Amazon Craton based on integration of field mapping and U-Pb and Sm-Nd geochronology. *Gondw. Res.* 3, 453–488.
- Santos, J.O.S., Potter, P.E., Reis, N.J., Hartmann, L.A., Fletcher, I.R., McNaughton, N.J., 2003. Age, source, and regional stratigraphy of the Roraima Supergroup and Roraima-like outliers in northern South America based on U-Pb geochronology. *Geol. Soc. Am. Bull.* 3, 331–348.
- Santos, J.O.S., Rizzotto, G.J., Hartmann, L.A., McNaughton, N.J., Fletcher, I.R., 2001. Ages of sedimentary basins related to the Sunsas and Jurueña orogenies, Southwest Amazon Craton established by zircon U-Pb geochronology. *Workshop Geology of the SW Amazonian Craton: State-of-the-Art*. São Paulo. Extended Abstract 114–118.
- Santos, J.O.S., Rizzotto, G.J., Potter, P.E., McNaughton, N.J., Matos, R.S., Hartmann, L.A., Chemale Jr., F., Quadros, M.E.S., 2008. Age and autochthonous evolution of the Sunsas Orogen in West Amazon Craton based on mapping and U-Pb geochronology. *Precamb. Res.* 165, 120–152.
- Schobbenhaus, C., Brito-Neves, B.B., 2003. A geologia do Brasil no Contexto da Plataforma Sul-Americana. In: *Bizzi, L. A., Schobbenhaus, C., Vidotti, R. M., Gonçalves, J. H. Geologia, tectônica e recursos minerais do Brasil: texto, mapas & SIG, Brasília, CPRM – Serviço Geológico do Brasil*, 692 p.
- Schobbenhaus, C., Campos, D. A. Derze, G. R., Asmus, H. E., 1984. *Geologia do Brasil: Texto explicativo do Mapa Geológico do Brasil e da área oceânica adjacente incluindo depósitos minerais*, escala 1:2.500.000. Brasília, DNPMP, 501p.
- Schobbenhaus, C., Gonçalves, J. H., Santos, J. O. S., Abram, M.B., Leão Neto, R., Matos, G. M. M., Vidotti, R. M., Ramos, M. A. B., Jesus, J. D. A., 2004. *Carta Geológica do Brasil ao Milionésimo*. Sistema de Informações Geográficas. Folhas Boa Vista (NA-20) e Roraima (NB-20). Escala 1:1.000.000. CPRM.
- Sécólo, D.B., Ruiz, A.S., Sousa, M.Z.A., Lima, G.A., 2011. Geologia, petrografia e geoquímica do enxame de diques máficos da região de Vila Bela da Santíssima Trindade (MT) – Suíte Intrusiva Huanchaca – SW do Cráton Amazônico. *Geociências, UNESP, São Paulo* 30 (4), 561–573.
- Slagstad, T., Kulakov, E., Kirkland, C.L., Roberts, N.M.W., Ganerød, M., 2019. Breaking the Grenville-Sveconorwegian link in Rodinia reconstructions. *Terra Nova* 31, 430–437. <https://doi.org/10.1111/ter.12406>.
- Smirnov, A.V., 2017. Intensity of Geomagnetic Field in the Precambrian and Evolution of the Earth's Deep Interior. *Phys. Solid Earth* 53 (5), 760–768. <https://doi.org/10.1134/S1069351317050123>.
- Sun, L., Wang, W., Lu, G., Xue, E., Huang, S., Pandit, M.K., Huang, B., Tong, X., Tian, Y., Zhang, Y., 2021. Neoproterozoic geodynamics of South China and implications on the Rodinia configuration: The Kunyang Group revisited. *Precamb. Res.* 363, 106338 <https://doi.org/10.1016/j.precamres.2021.106338>.
- Swanson-Hysell, N.L., Kilian, T.M., Hanson, R.E., 2015. A new grand mean palaeomagnetic pole for the 1.1 Ga Umkondo large igneous province with implications for palaeogeography and the geomagnetic field. *Geophys. J. Int.* 203, 2237–2247. <https://doi.org/10.1093/gji/ggv402>.
- Swanson-Hysell, N.L., Ramezani, J., Fairchild, L.M., Rose, I.R., 2019. Failed rifting and fast drifting: Midcontinent Rift development, Laurentia's rapid motion and the driver of Grenvillian orogenesis. *GSA Bull.* 131 (5/6), 913–940. <https://doi.org/10.1130/B31944.1>.
- Tassinari, C.C.G., Macambira M.J.B., 2004. A evolução tectônica do Cráton Amazônico. In: *Mantesso-Neto V., Bartorelli A., Dal Ré Carneiro C., Brito Neves B.B. (eds.) Geologia do Continente Sul-Americano: Evolução da obra de Fernando Flávio Marques de Almeida*. São Paulo, Ed. Beça, p. 471–485.
- Tassinari, C. C. G., Bettencourt, J. S., Gerales, M. C., Macambira, M. J. B., Lafon, J. M., 2000. The Amazonian Craton. In: *Cordani, U. G., Milani, E. J., Thomaz-Filho, A., Campos, D. A., (Eds), Tectonic Evolution of South America. Rio de Janeiro, 31st International Geological Congress*, p. 41–95.
- Tassinari, C.C.G., Macambira, M.J.B., 1999. Geochronological provinces of the Amazonian Craton. *Episodes* 22, 174–182.
- Teixeira, W., Gerales, M.C., Matos, R., Ruiz, A.S., Saes, G., Vargas-Mattos, G., 2010. A review of the tectonic evolution of the Sunsas belt, SW portion of the Amazonian Craton. *J. S. Am. Earth Sci.* 29, 47–60.
- Teixeira, W., Hamilton, M.A., Lima, G.A., Ruiz, A.S., Matos, R., Ernst, R.E., 2015. Precise ID-TIMS U-Pb baddeleyite ages (1110–1112 Ma) for the Rincon del Tigre-Huanchaca large igneous province (LIP) of the Amazonian Craton: Implications for the Rodinia supercontinent. *Precamb. Res.* 265, 273–285.
- Teixeira, W., Hamilton, M.A., Girardi, V.A.V., Faleiros, F.M., Ernst, R.E., 2019. U-Pb baddeleyite ages of key dyke swarms in the Amazonian Craton (Carajás/Rio Maria and Rio Apa areas): Tectonic implications for events at 1880, 1110 Ma, 535 Ma and 200 Ma. *Precamb. Res.* 329, 138–155. <https://doi.org/10.1016/j.precamres.2018.02.008>.
- Tohver, E., Van der Pluijm, B.A., Van der Voo, R., Rizzotto, G., Scandolaria, J.E., 2002. Paleogeography of the Amazon craton at 1.2 Ga: early Grenvillian collision with the Llano segment of Laurentia. *Earth Planet. Sci. Lett.* 199, 185–200.
- Tohver, E., Bettencourt, J.S., Tosdal, R., Mezger, K., Leite, W.B., Payolla, B.L., 2004a. Terrane transfer during the Grenville orogeny: tracing the Amazonian ancestry of

- southern Appalachian basement through Pb and Nd isotopes. *Earth Planet. Sci. Lett.* 228, 161–176.
- Tohver, E., van der Pluijm, B., Mezger, K., Essene, E., Scandolaro, J., 2004b. Significance of the Nova Brasilândia metasedimentary belt in western Brazil: redefining the Mesoproterozoic boundary of the Amazon craton. *Tectonics* 23, TC6004. <https://doi.org/10.1029/2003TC001563>.
- Tohver, E., van der Pluijm, B.A., Mezger, K., Scandolaro, J.E., Essene, E.J., 2005a. Two stage tectonic history of the SW Amazon craton in the late Mesoproterozoic: identifying a cryptic suture zone. *Precamb. Res.* 137, 35–59.
- Tohver, E., Van der Pluijm, B.A., Scandolaro, J.E., Essene, E., 2005b. Late mesoproterozoic deformation of SW Amazonia (Rondonia, Brazil): geochronological and structural evidence for collision with Southern Laurentia. *J. Geol.* 113, 309–323. <https://doi.org/10.1086/428807>.
- Tohver, E., Teixeira, W., van der Pluijm, B., Geraldés, M., Bettencourt, J.S., Rizzotto, G. J., 2006. Restored transect across the exhumed Grenville orogen of Laurentia and Amazonia, with implications for crustal architecture. *Geology* 34, 669–672.
- Van der Voo, R., 1990. The reliability of paleomagnetic data. *Tectonophysics* 184, 1–9.
- Veikkolainen, T., Pesonen, L.J., 2014. Palaeosecular variation, field reversals and the stability of the geodynamo in the Precambrian. *Geophys. J. Int.* 199 (3), 1515–1526. <https://doi.org/10.1093/gji/ggu348>.
- Wang, C., Mitchell, R.N., Murphy, J.B., Peng, P., Spencer, C.J., 2021. The role of megacontinents in the supercontinent cycle. *Geology* 49, 402–406. <https://doi.org/10.1130/G47988.1>.
- Yakubchuk, A.S., 2019. From Kenorland to Modern Continents: Tectonics and Metallogeny. *Geotectonics* 53 (2), 169–192. <https://doi.org/10.1134/S0016852119020109>.
- Zijderveld, J.D.A., 1967. A. C. demagnetization of rocks: analysis of results. In: Collinson, D.W., Creer, K.M., Runcorn, S.K. (Eds.), *Methods in Paleomagnetism*, pp. 254–286.